

Importance of Ice Nucleation and Precipitation on Climate with the Parameterization of Unified Microphysics Across Scales version 1 (PUMASv1)

Andrew Gettelman¹, Hugh Morrison¹, Trude Eidhammer¹, Kate Thayer-Calder¹, Jian Sun¹, Richard Forbes², Zachary McGraw^{3,4}, Jiang Zhu¹, Trude Storelvmo⁵, and John Dennis¹

¹National Center for Atmospheric Research, Boulder, CO, USA

²European Centre for Medium Range Weather Forecasts, Reading, UK

³Department of Applied Physics and Applied Mathematics, Columbia University, New York, NY, USA

⁴NASA Goddard Institute for Space Studies, NY, USA

⁵Department of Meteorology, University of Oslo, Oslo, Norway

Correspondence: A. Gettelman (andrew@ucar.edu)

Abstract. Cloud microphysics is critical for weather and climate prediction. In this work, we document updates and corrections to the cloud microphysical scheme used in the Community Earth System Model (CESM) and other models. These updates include a new nomenclature for the scheme, [now called Parameterization of Unified Microphysics Across Scales \(PUMAS\)](#), and the ability to run the scheme on Graphics Processing Units (GPUs). The main science changes include ~~removing~~ [refactoring](#) an ice number limiter and associated changes to ice nucleation, adding vapor deposition onto snow, and introducing an implicit numerical treatment for sedimentation. We also detail the improvements in computational performance that can be achieved with GPU acceleration. We then show the impact of these scheme changes on (A) mean state climate, (B) cloud feedback response to warming and (C) aerosol forcing. We find that corrections are needed to the immersion freezing parameterization ~~without a limit on ice number~~, [and that ice nucleation has important impacts on climate](#). We also find that the revised scheme produces less [cloud](#) liquid and ice, but that this can be adjusted by changing the loss process for cloud liquid (auto-conversion). Furthermore, there are few discernible effects of the PUMAS changes on cloud feedbacks, but some ~~significant~~ reductions in the magnitude of Aerosol Cloud Interactions (ACI). Small cloud feedback changes appear to be related to the implicit sedimentation scheme, with a number of factors affecting ACI.

1 Introduction

Cloud microphysics is critical for weather and climate. In particular, supercooled liquid water ([liquid at temperatures below 0°C](#)) and the fraction of condensate in the form of supercooled liquid at high latitudes has been shown to be important for mean state climate (Bodas-Salcedo et al., 2019) and weather (Forbes et al., 2015) biases. Supercooled liquid water is also important for understanding cloud feedbacks and climate sensitivity (Tan et al., 2016; Gettelman et al., 2019b; Tan and Storelvmo, 2019). For example, the Community Earth System Model version 2 (CESM2, Danabasoglu et al. (2020)) has been shown to have a higher supercooled liquid fraction than observed (Gettelman et al., 2020) which has been linked to a higher climate sensitivity

than previous versions (Gettelman et al., 2019b). In addition, cloud microphysics controls the formation of precipitation, which is often too light and too frequent in large scale weather and climate models (Stephens et al., 2010). This frequency bias has been shown to be directly attributable to cloud microphysics (Gettelman et al., 2021b)(Gettelman et al., 2021a). In this manuscript, we describe adjustments and corrections to the ice microphysics and precipitation process in an advanced cloud microphysics
25 scheme used in several global models and how these changes can have a significant effect on simulated climate.

The state of the art for global model cloud microphysics is the use of bulk two moment schemes, such as the scheme developed by Morrison and Gettelman (2008) (MG1). The CESM2 atmosphere model uses cloud microphysics described by Gettelman and Morrison (2015) and Gettelman et al. (2015), termed ‘MG2’ (Morrison-Gettelman version 2). The scheme has been updated further to include rimed ice by Gettelman et al. (2019a) (MG3). Most two moment bulk schemes utilize
30 classes of hydrometeors (such as cloud liquid, cloud ice, and snow). In such schemes, number and mass are predicted for each class and hydrometeors are treated using a size distribution with a fixed functional form. Two moment schemes are widely used in mesoscale models (Thompson and Eidhammer, 2014) (e.g., Thompson and Eidhammer, 2014) at resolutions of a few kilometers, but less commonly used in global models (e.g., Lohmann et al., 1999, 2007; Michibata et al., 2019). The scheme of Morrison and Milbrandt (2015) uses a single hydrometeor class to represent all ice particles, thereby unifying the treatment
35 of cloud ice and snow, and was implemented in the MG1 scheme by Eidhammer et al. (2016).

Our purposes in this manuscript are several. First, we document updates and corrections to the CESM2-MG3 cloud microphysical scheme used in CESM2. These include a new nomenclature for the scheme, and the ability to run the scheme on Graphics Processing Units (GPUs). We detail the improvements in computational performance that can be achieved with GPU acceleration. We then show the impact of the changes and corrections on (A) mean state climate, (B) cloud feedback
40 response to warming and (C) aerosol forcing. Note that we are not presenting a new set of tuned model configurations at this time. Rather, we show the impacts of changes and improvements in the scheme, particularly related to ice and mixed-phase processes, with the goal of building toward a cloud physics scheme that can work across scales (as shown in Gettelman et al., 2019c).

We describe the model and microphysics scheme updates in Section 2. Section 3 describes the methodology, simulations
45 and evaluation. Section 4 presents results, and Section 5 has discussion and conclusions.

2 Model Description

2.1 Model Description, CESM2

CESM2 (Danabasoglu et al., 2020) features the Community Atmosphere Model version 6 (CAM6) as its atmosphere model. CAM6 uses a two-moment stratiform cloud microphysics scheme MG2 (Gettelman and Morrison, 2015; Gettelman et al.,
50 2015) with prognostic liquid, ice, rain and snow hydrometeor classes. As a two-moment bulk scheme, MG2 has prognostic variables for number and mass mixing ratios for each of the hydrometeor classes. It also permits ice supersaturation and is described further below.

MG2 is also coupled to a 4-mode aerosol model (Liu et al., 2016) with liquid activation following Abdul-Razzak and Ghan (2002) and features natural and anthropogenic aerosols. CAM6 includes a physically based mixed phase ice nucleation scheme (Hoose et al., 2010) and accounts for preexisting ice for nucleation (Shi et al., 2015). MG2 is coupled to a unified moist turbulence scheme, Cloud Layers Unified by Binormals (CLUBB, Golaz et al., 2002; Larson et al., 2002), implemented in CAM by Bogenschutz et al. (2013). CLUBB treats boundary layer moist turbulence, stratiform clouds and shallow cumulus. CAM6 uses an ensemble plume mass flux deep convection scheme (Zhang and McFarlane, 1995; Neale et al., 2008) with simple microphysics. The radiation scheme is the Rapid Radiative Transfer Model for General Circulation Models (RRTMG) (Iacono et al., 2000).

2.2 Cloud Microphysics

MG2 (Gettelman and Morrison, 2015) is an update of the original MG scheme (Morrison and Gettelman, 2008; Gettelman et al., 2008). The original MG scheme was implemented in CAM5 as described by Gettelman et al. (2010). MG2 added prognostic rain and snow and is used in CAM6. Many of the process rate treatments are similar to the bulk two moment microphysics scheme of Morrison et al. (2005) developed for mesoscale models. Gettelman et al. (2019a) further updated the MG2 scheme to ‘MG3’ by adding rimed ice (with a switch to represent either graupel or hail). Thus, MG3 includes two additional prognostic variables for graupel/hail number and mass mixing ratios. In separate work, Eidhammer et al. (2016) and Zhao et al. (2017) updated the scheme to use a single category for cloud ice and snow. This has not been implemented yet in MG2 or MG3, and integration is a subject for future work.

Versions of MG microphysics have been adapted for use in the NASA-GEOS (Goddard Earth System Model for Earth Observation) model (Barahona et al., 2014), ~~The~~the Geophysical Fluid Dynamics Laboratory (GFDL) Atmospheric Model (AM) (Salzmann et al., 2010) and the NASA Goddard Institute for Space Studies (GISS) model (Cesana et al., 2019). The scheme is also available in the idealized Kinematic Driver (KID) (Shipway and Hill, 2012; Gettelman et al., 2019a). MG1 and MG2 are also used in a suite of earth system models derived from CESM1 and CESM2. Analyses have been conducted against observations for sub-grid process rate formulations (Lebsock et al., 2013) and against in-situ aircraft flights for supercooled liquid water (Gettelman et al., 2020). There has been significant work on numerical timestepping issues detailed by Gettelman and Morrison (2015) and Santos et al. (2020).

There are now a large number of people ~~are~~ contributing to community development of the MG scheme. Thus, the ‘MG’ name is no longer appropriate and we are now naming the scheme the Parameterization for Unified Microphysics Across Scales (PUMAS). This manuscript describes the updates and changes from MG3 to PUMAS (version 1).

As part of this update, we have tested and implemented several science and software changes to PUMAS beyond the MG3 scheme (Gettelman et al., 2019a). These changes are:

1. Refactoring of the ice number limiter.
2. ~~Reverting Immersion Freezing to Bigg (1953)~~Reduced aerosol number for ice nucleation.
3. Allowing vapor depositional growth of snow.

4. Fall speed correction for rain/snow/graupe.
5. An option for implicit sedimentation calculation.
6. An option for cloud droplet accretion by rain to act on newly autoconverted rain.
7. Addition of OpenACC (GPU accelerator) directives.
- 90 8. Optional switches to replicate processes in the European Centre for Medium Range Weather Forecasts (ECMWF) Integrated Forecast System (IFS).

2.2.1 Ice Number Limiter

In all versions of MG microphysics, a cloud-ice-number limiter is applied such that, when integrated over the time step, ice nucleation cannot increase the total ice concentration beyond the concentration of available ~~ice-nuclei~~ [Ice Nucleating Particles](#) (INP). This approach limits ice number from all processes except sedimentation and homogeneous freezing of cloud and rain drops. The concentration of available ~~ice-nuclei~~ INP in this approach, *NIMAX*, includes the Liu and Penner (2005) homogeneous *NIHOM* and heterogeneous *NIHET* cirrus ice nucleation and the empirical Meyers et al. (1992) ice nucleation as a function of temperature for the mixed phase *NIMEY*:

$$NIMAX = NIHET + NIHOM + NIMEY \quad (1)$$

100 When the Hoose and Möhler (2012) Classical Nucleation Theory (CNT) based scheme was introduced in CAM6 and the Meyers et al. (1992) ice nucleation removed, the ice nucleation source from Hoose and Möhler (2012) *NICNT*, comprising immersion, deposition and contact freezing terms, was not added to *NIMAX* (the equation above was unchanged). In addition, the ice nucleation source from Meyers et al. (1992) was set to zero ($NIMEY = 0$). As a result *NIMAX* in the mixed phase regime (where $NICNT > 0$) is too low, preventing the model from adding ice crystals through local nucleation as intended.

105 The reduced *NIMAX* leads to lower ice number concentration, and hence increased size and increased fall speed and loss through sedimentation (~~Shaw et al., 2021~~) ([Shaw et al., 2022](#)) as well as affecting the balance of ice and supercooled liquid at high latitudes. In CAM6, this increases the supercooled liquid fraction when the *NIMAX* limiter is removed (~~Shaw et al., 2021~~) ([Shaw et al., 2022](#)). The CAM6 simulated supercooled liquid fraction is higher than observed in key regions (Gettelman et al., 2020). The supercooled liquid fraction and ice nucleation have been implicated in altering cloud feedbacks and climate sensitivity (Gettelman et al., 2019b; Tan and Storelvmo, 2019), suggesting that how the ice number limiter is applied may be important.

In this update (all simulations but the ‘control’), the *NIMAX* limiter on ice nucleation has been removed and instead an overall cap on in-cloud ice number concentration is added to the end of the microphysics (set at 100 cm^{-3}) ~~to represent a maximum~~ [typical ice crystal number found in deep clouds](#)). [At small scales measurements have shown much higher concentrations, up to \$\sim 50 \text{ cm}^{-3}\$, embedded within broader regions with much lower concentrations \$< 1 \text{ cm}^{-3}\$ \(e.g., \(Hoyle et al., 2005\)\).](#) Satellite

retrievals also show lower concentrations (up to several hundred per liter) over broad regions, e.g. (Gryspeerd et al., 2018). The main point is that we want to set this upper limit for ice concentration NIMAX to a large value such that it encompasses the range of physical values – in general we want the process parameterizations to control the ice concentration rather than NIMAX, and only impose the limit to ensure values are within a physically reasonable range. This is similar to the ice number concentration limiter applied to many two-moment microphysics schemes in cloud and mesoscale models (Morrison et al., 2005; Milbrandt and Yau, 2005; Thompson and Eidhammer, 2014). Zhu et al. (2022) implemented a similar change to develop a version of CESM2 for use in paleoclimate applications.

2.2.2 ~~Reverting Immersion Freezing~~ Reduced Aerosol Number for Ice Nucleation

When the ice number limiter is ~~removed~~refactored, the immersion freezing component of the ~~classical nucleation theory~~ Classical Nucleation Theory (CNT) mixed phase ice nucleation scheme of Hoose et al. (2010) was found to produce an unrealistically high number of ice crystals near the low end of the mixed phase temperature range (-38°C), heavily concentrating ice crystals in the mid-to-upper atmosphere near desert regions (sources of mineral dust that acts as ice nucleating particles) to an extent not evident in satellite retrievals (Sourdeval et al., 2018)(Sourdeval et al., 2018; McGraw et al., 2022). Figure 1C-B illustrates the large increase in ice number when PUMAS is implemented with the original MG2 CNT immersion freezing. ~~As a result, this component of the CNT mixed phase ice nucleation is switched off, reverting to the empirical treatment of Bigg (1953) used in MG1 which depends on temperature and cloud drop size (MG2 Imm). Accordingly we make two adjustments to the scheme to reduce aerosol number (particularly dust) involved in ice nucleation. First, instead of calculating the number fraction for dust and BC based on observed field measurements of dust size distributions, we calculate the number fraction from the mass fraction of the aerosols for immersion freezing. Second, we allow only a fraction of the dust to nucleate (5%), similar to what is already done for black carbon (1% used), following McGraw et al. (2022). The results are illustrated in Figure 1C, not the presence of aerosol particles. The use of Bigg (1953) immersion freezing does not represent the strong dependence of ice nucleation on proximity to mineral dust sources seen with the current CNT implementation. This may represent mixed-phase clouds more like in the real world, where ice at mixed-phase temperatures can additionally nucleate on aerosol species not included in CESM, such as bioaerosols (Kanji et al., 2017). The ice number difference relative to CAM6 goes away if the Bigg (1953) parameterization for immersion freezing of cloud drops is used in PUMAS (number concentrations look more similar to the control simulation (note that the difference scale is a factor of 10 lower in Figure 1B)C than in Figure 1B), but there still is some immersion freezing active (see below).~~ A complete explanation for the excessive ice nucleation at the edge of the applied temperature range for CNT is a subject of future work. However, one possibility is that without considering a full aerosol budget that removes cloudborne aerosols, CNT results in excessive nucleation and high ice numbers. This will influence the simulations described in Zhu et al. (2022), wherein CNT without an ice number limiter was shown to produce improvements in paleoclimate simulations though very possibly at the expense of realistic mixed-phase clouds and associated feedbacks. The overactive CNT nucleation may also have enabled the strong sensitivity to numerical sub-stepping of the microphysics in that study's model version.

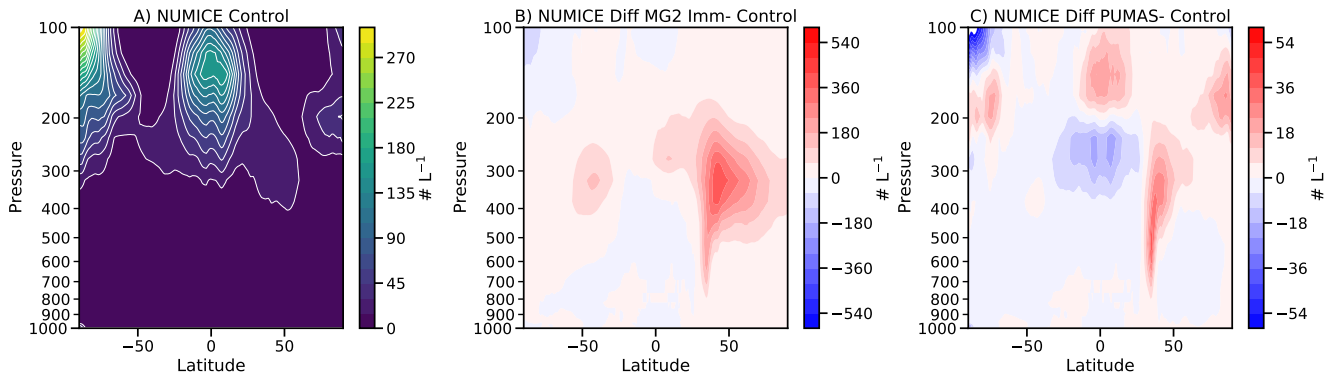


Figure 1. Zonal annual mean latitude height plots of A) Cloud ice number (NUMICE) from the MG3 Control simulation, B) [PUMAS-MG2 Immersion Freezing \(no immersion limits in CNT dust\)](#) - Control difference, and C) [PUMAS-Imm \(CNT Immersion Freezing\)](#)-PUMAS - Control difference. [Note the difference in scales between B and C.](#)

2.2.3 Vapor Deposition onto Snow

150 All versions of MG include vapor deposition onto ice in ice supersaturated conditions, but not vapor deposition onto snow. For physical consistency, we have now added [in PUMAS](#) vapor deposition onto snow [in PUMAS, both for mass and number mixing ratios](#). This follows the same method as for vapor deposition onto cloud ice as described in Morrison and Gettelman (2008), equations 21-22, but uses snow size distribution parameters instead. Grid mean temperature, humidity and snow [mass](#) mixing ratio are used in the calculation. The calculation is limited to prevent over-depletion of ice supersaturation (conditions cannot become ice sub-saturated from vapor deposition).

155

2.2.4 Precipitation Fall Speed

In the MG1, MG2, and MG3 parameterizations, sedimentation of all cloud and precipitation categories is sub-stepped to maintain numerical stability for the explicit first-order upwind calculation. Precipitation has zero fall speed if it hits a level with no precipitation during a sedimentation sub-step. This will result in “stalling” of the precipitation for the remainder of the full (not sub-stepped) time step. This can be a problem with long time steps (the standard CESM2 physics timestep is 1800s).

160 We have implemented a correction which sets the number- and mass-weighted fall speeds for each hydrometeor category to that at the lowest level that contains non-zero ([mixing ratio larger than 1.e.mass mixing ratio with respect to dry air larger than \$10^{-10}\$](#)) mass of that category before the sub-stepping and sedimentation calculation. Thus, number and mass for that category will fall at constant speeds below the lowest model level with non-zero category mass.

165 2.2.5 Implicit Sedimentation

The default method used for sedimentation in all MG versions is an explicit first-order upwind calculation. Sedimentation sub-steps the timestep to ensure numerical stability with the fall velocity. We have added an option for a time-implicit monotonic scheme for sedimentation using a single fall speed profile. The calculation is from Guo et al. (2021) Appendix A. The hydrometeor number and mass mixing ratio q of a hydrometeor class at the $n + 1$ time step and the k vertical layer (q_k^{n+1}) is

170 are defined by (Guo et al., 2021, equation A3):

$$q_k^{n+1} = \frac{q_k^n \delta z_k + q_{k-1}^{n+1} v_{k-1} \delta t}{\delta z_k + v_k \delta t} \quad (2)$$

where δt is time step, v is the number or mass weighted mean fall velocity, and δz_k is the depth of the k -th vertical layer. Note that k increases downward so the flux is dependent on what is above, and the fall speed correction will have no or little impact. The implicit scheme was originally derived from the GFDL microphysics (appendices in Harris et al. (2020) and Zhou et al. (2019)), and reduces sensitivity to time step without sub-stepping (see section 4.2). This approach is less accurate (more diffusive) at the gain of being much faster, as shown by Guo et al. (2021). In Section 4.2, we will show it does not introduce significant errors in the solutions.

2.2.6 Modification of Accretion

The autoconversion parameterization in MG and PUMAS is from Khairoutdinov and Kogan (2000) (KK2000). The KK2000 autoconversion to rain tendency ($\Delta q_r = -\Delta q_c$) is a function of condensate, the change in mass mixing ratio (q_c) and number concentration (N_c), while accretion is a function of q_c and rain mass mixing ratio (q_r) per second, is defined as:

$$\Delta q_{r,AUTO} = A q_c^B n_c^C \quad (3)$$

where $A=13.5$, $B=2.74$ and $C=-1.1$. Accretion (an additional Δq_r) is defined as:

$$\Delta q_{r,ACCRES} = A (q_c q_r)^B \quad (4)$$

185 where $A=67$ and $B=1.15$. In principle, if there is autoconversion in a long time step, autoconverted rain (q_r) may accrete cloud liquid. We experiment to see if this affects the This change may impact aerosol-cloud interactions by allowing accretion to operate on the newly autoconverted rain, but by adding it to the existing rain mass for the evaluation of accretion—calculation of accretion so it becomes:

$$\Delta q_{r,ACCRES} = A ([q_c - \Delta q_{r,AUTO}] [q_r + \Delta q_{r,AUTO}])^B \quad (5)$$

190 This allows accretion to occur during the same time step as initial rain formation from autoconversion. We hypothesize that this may increase the accretion to autoconversion ratio and that might impact the indirect aerosol forcing (Gettelman, 2015).

2.2.7 GPU Directives

The atmosphere model consists of many parameterizations whose calculations are grid-independent or column-independent. Therefore, it is possible to achieve massive parallelism for a parameterization by carefully restructuring the code and increasing the number of columns (for a global model, this means increasing the horizontal resolution), which then becomes a natural fit for GPU computing (Sun et al., 2018).

In this study, the PUMAS code is GPU-enabled by using the OpenACC directives, which allows the same source code to run on either CPU or GPU and keep its maintainability. The test machines used in this paper are Cheyenne (<https://www2.cisl.ucar.edu/resources/computational-systems/cheyenne>) and Casper (<https://www2.cisl.ucar.edu/resources/computational-systems/casper>) at NCAR. Cheyenne is a homogeneous cluster with CPU-based nodes only, while Casper is a heterogeneous cluster with the NVIDIA V100 GPUs available on some compute nodes. The performance comparison below is made between one full CPU node on Cheyenne/Casper (i.e., 36 CPU cores) and one V100 GPU on Casper. We limit the simulation length to 1 day, which we find is long enough to show the performance difference. We mainly measure the timing information of the calculations within PUMAS and report the maximum wall-clock time among the MPI processes that is averaged over the simulation length and sub-cycles (there is by default 3 sub-steps per time step for the calculation of MG2 tendency using the 1-degree resolution). For the GPU simulation, we also measure the timing information of GPU computations and data copy between the CPU (i.e., host) and GPU (i.e., device) and GPU internal memory allocation to better illustrate their relative computational cost. Last but not the least, we vary the maximum number of atmospheric columns per single processing element (called a ‘chunk’), the CAM PCOLS parameter. As noted by Worley and Drake (2005), there can be multiple chunks per MPI process. PCOLS is varied from 16 (the default value) to 1536 (the theoretical maximum number for 1-degree resolution and 36 MPI processes) to reveal its impact on the CPU and GPU performance.

Figure 2 shows the computational time of CPU and GPU for PUMAS without graupel. The figure compares computational times with increasing values of PCOLS. The newer Intel Skylake processors on Casper slightly outperform the previous generation Intel Broadwell processors on Cheyenne. In addition, the CPU runs consistently show longer computational time with respect to increased PCOLS, which is likely a penalty caused by lack of cache for a larger chunk size. In contrast, the GPU run is significantly slower than the CPU run when PCOLS = 16 and more than half of the time is spent on the computation (shown by pink bars). When PCOLS increases, more data is copied from CPU to GPU each time, meaning a higher parallelism and fewer total kernel launches on the GPU, as well as less frequent data movement between CPU and GPU. All of these factors contribute to the rapid decrease of computational time for the GPU run with larger PCOLS. A factor of $2\times$ to $3\times$ total speedup for the GPU relative to CPU is observed when PCOLS = 1536. This suggests that we should expect to benefit from GPU computing only when our problem size (i.e., number of columns per GPU) is large enough. We also notice that the data movement could be more costly than computation for a smaller chunk size. Porting additional CAM physics parameterizations that use the same data to the GPU would likely reduce relative cost of data movement and result in even more effective speedups. Even at PCOLS = 1536 the data transfer time is larger than the total computation time in Figure 2.

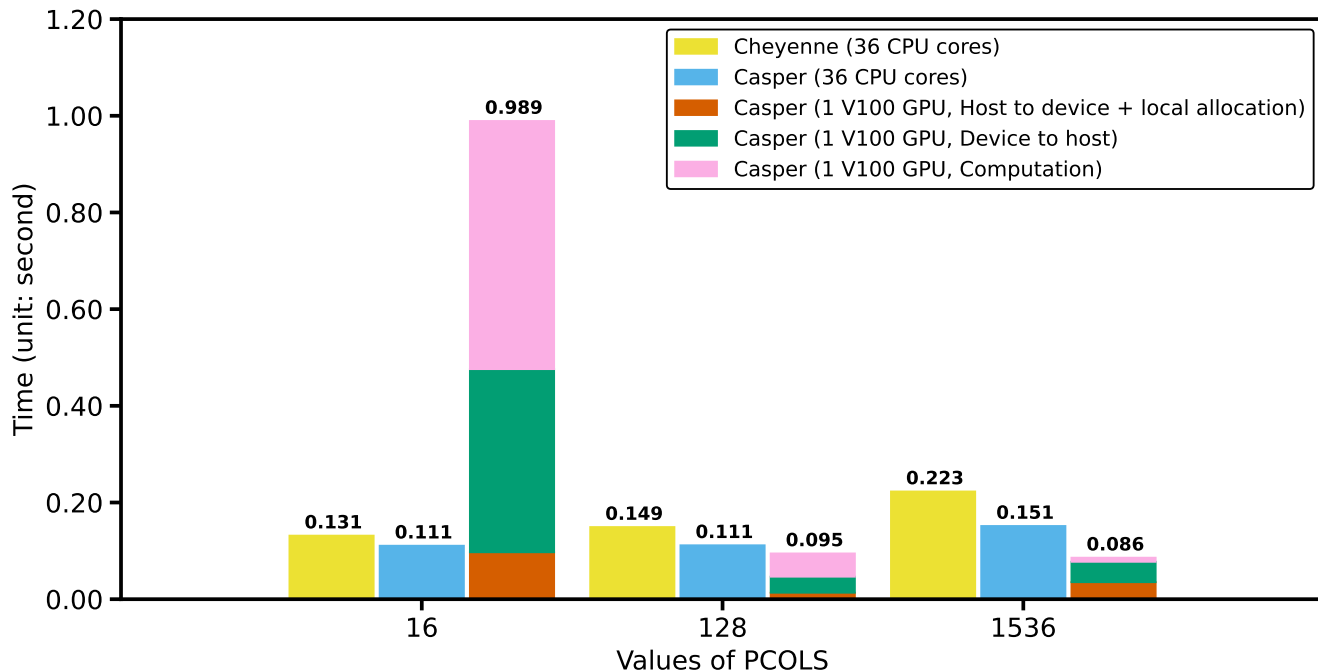


Figure 2. Averaged GPU-enabled MG2 run time per sub-step for different configurations on CPU and GPU. The computational time on GPUs is further divided into time spent copying data from the host to the device, from the device back to host, and time spent in pure computation. Simulations are performed on the Cheyenne and Casper computer system with details described in Section 2.2.7

225 The encouraging results here serve as a proof of concept for porting PUMAS to GPU. A separate manuscript ~~is under~~
~~preparation to~~ [has been submitted \(Sun et al, Accelerate the Parameterization of Unified Microphysics Across Scales \(PUMAS\)
on the graphics processing unit \(GPU\) with directive-based methods, submitted to Journal of Advances in Modeling Earth
Systems, 2022\) to](#) describe the technical details on porting PUMAS to GPU, optimizing the implementation and evaluating the
CPU and GPU performance with different configurations.

230 The addition of OpenACC directives is included in all the PUMAS tests, but does not change scientific results as it results
in only round off level changes.

2.2.8 Additional Switches

In a paper in preparation (Gettelman, et al [20222023](#), in preparation), an additional series of options were added to the PUMAS
scheme to adjust the fall speed, evaporation rate of cloud liquid and sedimenting condensate, and ability to use different ice
235 nucleation options. The changes enhance portability, and enable the PUMAS code to run in the ECMWF IFS system. This
code is currently available in the PUMAS github repository, but detailed in other work.

3 Methodology

Our analysis looks at the impact of the changes described in section 2 on the mean state present day climate, as well as the implications for climate forcing and climate feedbacks. Cloud microphysics impacts the forcing of climate via interactions with aerosol particles in the atmosphere that change cloud condensation nuclei (CCN), as first noted by Twomey (1977). This has significant possible feedbacks on cloud drops and radiation, as recently reviewed by Bellouin et al. (2020). Cloud microphysical responses to increased CCN and ice nucleus (IN) concentrations are a critical forcing agent for climate. Furthermore, clouds respond to the environmental state when the planet warms due to other factors (such as [the increase in anthropogenic greenhouse gases](#)). These cloud feedbacks are the largest uncertainty in determining the climate sensitivity – the response of the climate system to an imposed forcing (e.g., [Gettelman et al., 2016](#); [Sherwood et al., 2020](#)) (e.g., [Gettelman et al., 2016](#); [Zelinka et al., 2020](#); [Sherwood et al., 2020](#)). We assess how both aerosol forcing and climate feedbacks change due to changes in the cloud microphysics with detailed simulations and analysis.

3.1 Simulations

We conduct several 6 year long simulations using near present day cyclic boundary conditions for the year 2000. ~~This includes averaged levels of greenhouse gases and atmospheric oxidants.~~ [Boundary conditions used to force the model are climatological monthly averages over 1995–2000, including greenhouse gases, atmospheric oxidants](#) and emissions of aerosols ~~for the period 1995–2005.~~ [The climatological annual cycle is repeated each year.](#) We also use averaged Sea Surface Temperatures (SSTs) from observations (Hurrell et al., 2010). Data are compiled monthly and smoothly interpolated between months. Model resolution for CAM6 is 0.9° lat x 1.25° longitude with 32 levels in the vertical up to 10 hPa and a standard physics timestep of 1800s, and 3 coupling periods between microphysics and cloud ‘macrophysics’ (turbulence and large scale condensation), for a default microphysics timestep of 600s. Six years is sufficient that the differences between past, present and future configurations (see below) are much larger than the inter-annual standard deviation of global quantities (e.g. the signals are larger than internal variability).

For each of the cases described below in Section 3.1 we conduct the following experiments. The first is a simulation with Present Day (PD, year 2000) boundary conditions including SSTs, Greenhouse Gases (GHGs) and aerosol emissions. Next, we conduct simulations with (A) 1850 estimated aerosol emissions, termed ‘Pre-Industrial’ (PI) and (B) SST increased uniformly by +4K (SST4K). All other boundary conditions (especially ~~GHGs and SSTs~~) are the same. When compared with the PD simulation, PI assesses the impact of aerosol forcing, and SST+4K assesses the impact of cloud feedbacks, being representative of the full model response to warming as first noted by Cess et al. (1989), and verified for CESM2 by Gettelman et al. (2019b).

For detailed analysis, we also conduct single column model simulations with the Single Column Atmosphere Model (SCAM) that is available as a part of CAM (Gettelman et al., 2019c). SCAM runs exactly the same atmospheric physics parameterization code as the full 3D simulations. We focus on the Atmospheric Radiation Measurement (ARM) program June 1997 case for a month over the central great plains (Oklahoma, USA) called the ‘ARM97’ case, as well as the Mixed Phase Clouds Experiment

(MPACE) case from October 2004 over the North Slope of Alaska. Cases are detailed in Gettelman et al. (2019c). The standard
270 timestep in SCAM is 1200s, with 4 microphysics sub-steps for a microphysics timestep of 300s.

4 Results

3.1 Description of Sensitivity Tests

Sensitivity tests are grouped sequentially as indicated in Table 1, testing many of the items listed in Section 2.2, and with the
item numbers listed in that section. The first is a ~~control~~Control case, using the standard CAM6 and the MG3 microphysics. All
275 of these tests include graupel. ~~Beyond the control case~~Next, we test ~~all the a~~‘PUMAS’ modifications case with modifications
#1-7 listed in section ~~2.2- 2.2~~ except #8 (optional switches to replicate processes in the ECMWF IFS). This includes (1)
refactoring the ice number limiter, (2) reduced aerosol number for ice nucleation, (3) allowing vapor depositional growth of
snow, (4) fall speed corrections, (5) implicit sedimentation, (6) accretion seeing newly autoconverted rain and (7) addition of
ACC directives. An additional modification is to increase the specified diameter of ice crystals detrained from deep convection
280 from 25 to 60 μm (‘Control-Di60’). We test the impact of this change in a separate simulation based on the ~~control~~Control case.
The PUMAS simulation where we ~~do not use the Bigg (1953) immersion freezing, and instead use the CAM6 CNT version~~
use the CNT immersion freezing without reduced aerosol number acting as INPs (#2), is illustrated in Figure 1 (‘PUMAS-
Imm’). We then look at the impact of removing vapor deposition onto snow (#3) in PUMAS as described in Section 2.2
(‘PUMAS-VapDepSn’). Next, we test removing the fall speed modifications (#4) and implicit sedimentation (#5) in PUMAS
285 simulations in the ~~‘PUMAS-Implicit~~PUMAS-Fall’ simulations. Because the fall speed modifications mainly impact the explicit
rather than implicit treatment of sedimentation, we also tested the fall speed modifications alone with the explicit sedimentation
in PUMAS (e.g., testing explicit sedimentation with the fall speed correction). The results are basically the same as explicit
sedimentation without the fall speed correction in ~~PUMAS-Implicit~~PUMAS-Fall (not shown), indicating that the fall speed
correction has little impact. Finally, we also explore a simulation where we adjust (‘tune’) uncertain microphysical parameters
290 to increase cloud water and ice to get close to the ~~control~~Control case (‘PUMAS-Tune’). This tuning is accomplished by
scaling the autoconversion of cloud to rain by a ~~further~~ factor of 0.5 from the ~~control~~Control case and increasing the ~~size~~
~~threshold~~threshold diameter for ice autoconversion to 1000 μm (from the ~~control~~Control value of 500 μm).

4 Results

4.1 Process Rates

295 To look in detail at the effects of changes to the microphysics scheme, we focus on single column (SCAM) simulations for
the ARM97 summer case. Figure 3 illustrates Liquid (A-C), Ice (D-F), Rain (G-I) and Snow (J-L) process rates. Graupel was
included in these simulations but is not shown and discussed briefly below. The left column of Figure 3 (A,D,G,J) is the ~~control~~
Control simulation, the center column (B,E,H,K) is the ‘PUMAS’ modified code (changes #1–7 from Section 2.2) and the right

Table 1. Description of the simulations. Numbers in the options column correspond to the changes listed in Section 2.2.

Name	Options	Description
Control	None	Baseline CAM6 with MG3
Control-Di60	None	CAM6-MG3 with detrained ice size = 60 μm
PUMAS	#1-7	New Ice Limit + Vap Dep Snow + Fall speed + Accretion
PUMAS-Imm #1,3-7 PUMAS with the CAM6-CNT scheme	PUMAS-VapDepSn	#1-2,4-7 PUMAS without vapor deposition onto snow
PUMAS-Implicit PUMAS-Fall	#1-3,6-7	PUMAS without sedimentation and fall speed modification
PUMAS-Tune	#1-7	PUMAS + tuning to improve energy balance

column (C,F,I,L) the difference between the two. Differences in liquid at ~~high altitudes~~ pressures less than 600hPa mainly come from changes in ice and mixed-phase phase processes (vapor deposition). In particular there is less accretion of liquid onto snow (blue dot-dash line) and vapor deposition onto snow (~~Berg-Snow~~ Bergeron Snow, solid teal line), reducing the liquid loss rates at higher altitudes. At lower altitudes (pressures > 600 hPa) there are small changes to liquid, with less ~~sedimentation~~ liquid sedimentation (solid blue line) and more loss from accretion of cloud by rain (Accretion, dashed turquoise line).

Ice microphysics sees larger changes, with a decrease in ice mass loss from sedimentation (solid blue line), leading to a positive net change. This is caused by larger ice number from removing the NIMAX limiter, and results in more ice (~~and hence an increase in the melting source of liquid~~) mass. Cloud ice remaining longer in the atmosphere increases the availability for ~~vapor deposition~~ sublimation and deposition (dot-dash red) as well.

Precipitation changes in Figure 3 are also significant. Rain has a negative sedimentation tendency (solid blue line) all the way to the surface in the revised code (Figure 3H), with reduced fall speeds higher up. Snow has a positive sedimentation tendency (solid blue line) from 800–600hPa as snow falling from above enters a layer below. In PUMAS this continues all the way to the surface (Figure 3K) because the nonzero ~~fallspeed~~ fall speed was added below the lowest level of precipitation. The implicit sedimentation does not seem to introduce any numerical issues with rain or snow.

Graupel changes (not shown) ~~are modest~~ do not significantly affecting snow or other hydrometeors, and come mostly from differences in the graupel collecting snow term (dashed turquoise line), which is larger (more negative) in PUMAS (Figure 3L).

We have explored in detail how the different parts of the PUMAS code create these differences by plotting some of the changes separately (not shown). The upper level increases in cloud ice deposition and sublimation come from the ice number limiter change. The limiter also reduces low level accretion of cloud liquid (q_c) to rain (q_r) and snow (q_s). The implicit sedimentation results in more accretion of cloud liquid. The new accretion increases the accretion of cloud liquid as well, but reduces cloud ice deposition/sublimation. Thus, not all the changes act in the same way. The changes due to accretion including newly autoconverted rain have a smaller impact (limited to increasing low level accretion) than the explicit sedimentation or ice limiter changes.

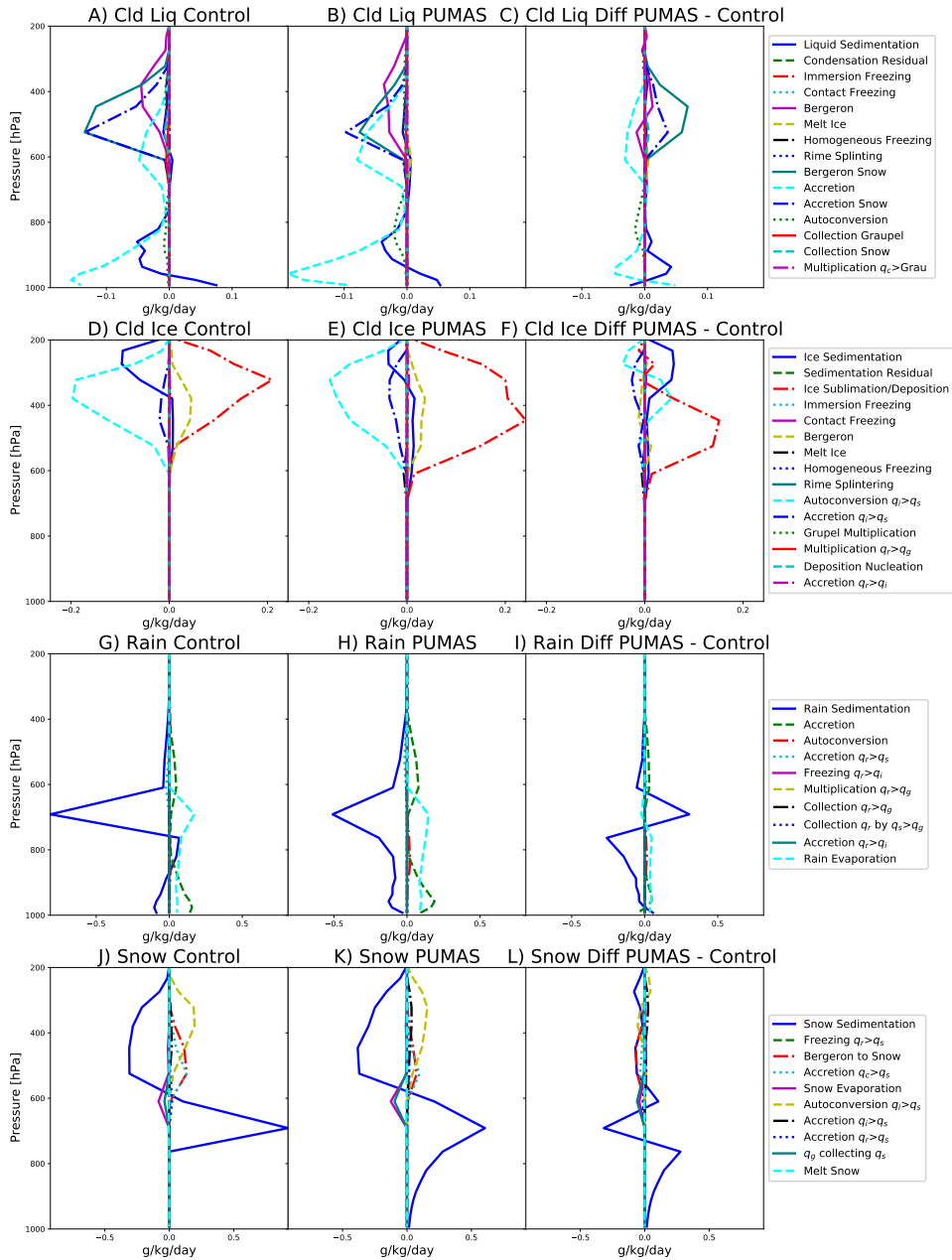


Figure 3. Mass mixing ratio process rate profiles from single column model (SCAM) simulations. Left column (A,D,G,J) is the MG3 Control simulation, the center column (B,E,H,K) the PUMAS code (Table 1, changes #1–7) and the right column (C,F,I,L) the difference. Top row (A,B,C) shows results for cloud liquid, then cloud ice (D,E,F), rain (G,H,I) and snow (J,K,L).

4.2 Timestep Sensitivity

We have also used the SCAM cases as a way to explore the time step sensitivity of the schemes. To focus on the microphysics, we set a 1200 s physics timestep in SCAM, with 4 sub-steps for the CLUBB unified turbulence scheme. We then can sub-step the microphysics within that 300 s sub-step. This takes the same condensation from turbulence and passes it to the microphysics, which we run from 300 s to 10 s (e.g., 1 to 30 microphysics-sub steps). The results are illustrated in Figure 4 for the June 1997 ARM97 case. We focus on the ~~control~~Control case (MG3), all the PUMAS modifications (PUMAS) and the PUMAS without the implicit sedimentation and fall speed corrections (~~PUMAS-Implicit~~PUMAS-Fall). Other sensitivity cases are similar to PUMAS. Figure 5 illustrates the same tests but for the Mixed Phase Clouds Experiment (MPACE) in October 2004 over the North Slope of Alaska.

Several results stand out. First, cloud liquid and rain (Figure 4 A and D) are fairly sensitive to time step changes for the SCAM ARM97 case in the ~~control~~Control (MG3) configuration. The same is true for supercooled liquid (Figure 4C). The PUMAS code reduces the timestep sensitivity of most of the ~~hydrometers~~hydrometeors. This is particularly true for the MPACE case in Figure 5, where cloud (Figure 5A) and supercooled liquid, (Figure 5C) as well as cloud ice ~~has~~have much less variability across timesteps than in the ~~control~~Control MG3 case. Most of this improvement is not seen if the fall speed and sedimentation changes are removed, indicating that implicit sedimentation contributes substantially to the reduced sensitivity of solutions to timestep (as expected). Figures 4B and C indicate reductions in supercooled liquid water and ice with the microphysical changes in PUMAS.

Impacts of the implicit sedimentation and fall speed changes are seen in the rain mass (Figure 4D). The peak rain mass for PUMAS in the ARM97 case is less variable in PUMAS than with the Control or PUMAS without implicit sedimentation. However, there is a reduced gradient below the peak for PUMAS, which may be caused by the more diffusive nature of the formulation. This is not an issue in the MPACE case (Figure 5D). It is not seen to be a problem in the 3D simulations.

The MPACE case (Figure 5) has less sensitivity to time step than ARM97 for the ~~control~~Control MG3 case, and even less sensitivity for PUMAS. Reduced sensitivity in all cases may have to do with the absence of deep convective cloud and deeper cloud in the MPACE while such cloud is present throughout the column in ARM97. Cloud liquid (all supercooled, Figure 5A and C) has little sensitivity in PUMAS, less than with MG3 or PUMAS-Implicit, again indicating the importance of implicit sedimentation. There is less cloud ice (Figure 5B) but more snow in the PUMAS simulations compared to MG3. Overall, besides the reduced time step sensitivity, PUMAS and ~~PUMAS-Implicit~~PUMAS-Fall give similar results for these SCAM cases.

4.3 Mean State Climate

Figure 6 illustrates zonal mean climatologies from 8-6 year global simulations of CAM6 with control microphysics (MG3) and updated PUMAS code. Also shown are observations of radiative fluxes and clouds from CERES satellite Energy Balance Adjusted Flux (EBAF) products (Loeb et al., 2018), Liquid Water Path (LWP) from the CERES SYN product (Rutan et al., 2015), and precipitation from the Global Precipitation Climatology Project (GPCP, (Adler et al., 2018)). We test the code following

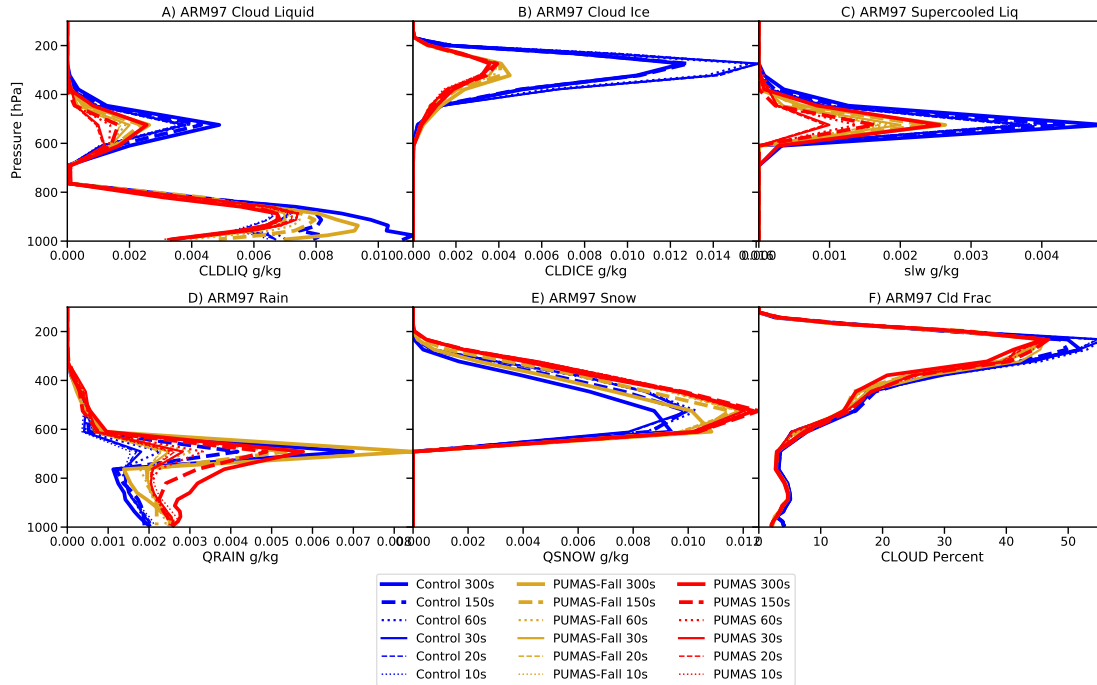


Figure 4. Time averaged single column model (SCAM) profiles from the ARM97 case with different time steps as indicated in the legend. Blue: MG3 Control cases, Orange: PUMAS-Implicit, Red: PUMAS. Simulation names are defined in Table 1. Results are shown for A) cloud liquid, B) cloud ice, C) supercooled liquid, D) rain, and E) snow mass mixing ratios and F) cloud fraction. Thicker lines indicate longer timesteps.

355 the experiments in Table 1. PUMAS (Blue) is the full set of modifications. PUMAS-VapDepSn (GreenOrange) removes vapor deposition onto snow, PUMAS-Implicit-OrangePUMAS-Fall (Green) removes the fall speed changes and uses an explicit rather than implicit sedimentation calculation, and PUMAS-Tune (Red) increases liquid and ice mass with parameter changes. The full PUMAS ice modifications (Blue) reduce the overall Cloud Radiative Effect (CRE) magnitude (less negative Shortwave [SW] and less positive Longwave [LW]) from the control-Control MG3 case by about 2.5 Wm^{-2} (Figure 6 G and H). The difference tends to reduce SW biases but increase LW biases with respect to CERES. This is due to lower LWP (Figure 6A) and IWP-ice Water Path (IWP) (Figure 6B). Cloud fraction, cloud top liquid number and precipitation (Figure 6C,D and F) are similar across all simulations. The PUMA-Tune-Note that the satellite data for LWP (Figure 6A) and cloud fraction (Figure 6C) (based on CERES and MODIS clouds) is not reliable at high southern latitudes over the ice sheet. It is clear that the highest water contents are NOT over the S. Pole. The PUMAS-Tune case is designed to increase liquid and ice (Figure 6A and B) to increase the magnitude of the cloud radiative effects so they are more similar to the control-Control (Figure 6G and H),

365

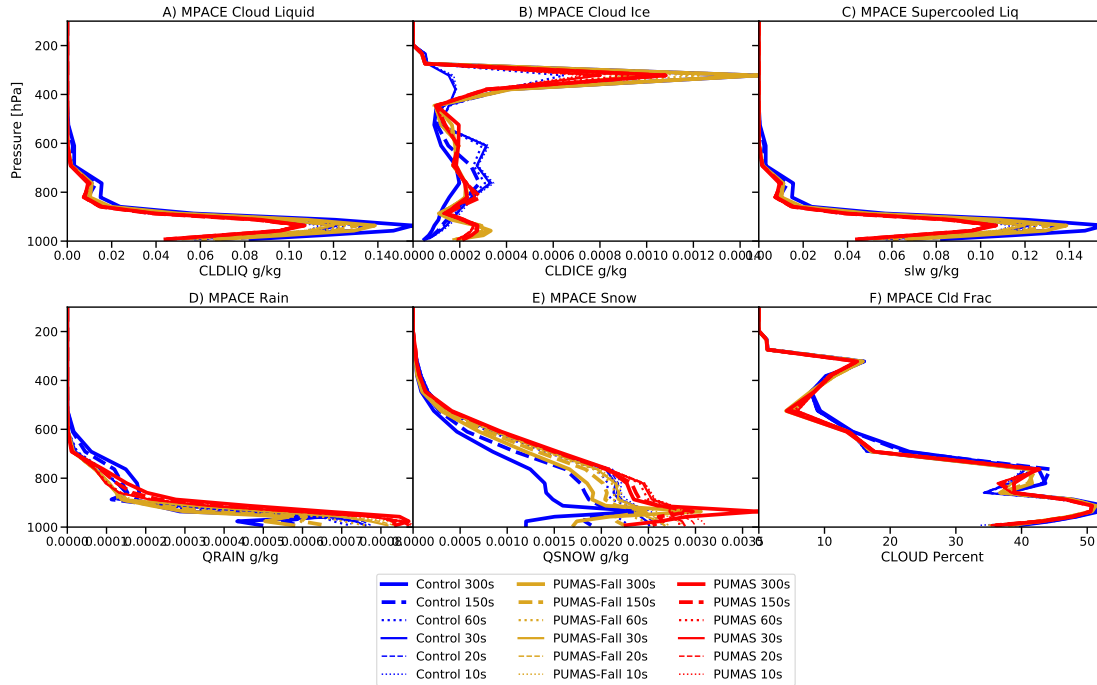


Figure 5. As in Figure 4 except for the MPACE case.

but it also decreases ice number (Figure 6E). The resulting cloud radiative effects (Figure 6G and H) are of lower magnitude than CERES LW observations, but generally within the variability of the observations (purple shading). Note the change to detrained ice size (included in all PUMAS simulations) is tested on [it's-its](#) own with the control model (Control-Di60), and it increases LWP (Figure 6A) and decreases IWP (Figure 6B), likely through faster sedimentation of larger ice crystals. [Also](#)
 370 [note that the revised immersion freezing \(present in all the PUMAS simulations, have higher ice numbers \(Figure 6E\) from 30–60°N latitude.](#)

Figure 7 illustrates ice fraction in the Control and PUMAS simulations. Ice fraction is calculated at each location and timestep as the ice [mass](#) mixing ratio divided by the total cloud water (ice and liquid) [mass](#) mixing ratio. An increase in ice fraction reduces the CRE from supercooled liquid water but increases CRE from ice. Cloud ice provides a negative cloud
 375 phase feedback when it is reduced under climate warming. The detrained ice size change does not impact the ice fraction in the [control-Control](#) simulation (Figure 7B). PUMAS features an increase in ice fraction in the tropical middle troposphere (600–300 hPa) relative to the MG3 Control simulation (Figure 7C). It appears that the implicit sedimentation change is the reason, as removing the implicit sedimentation [and the fall speed correction](#) (Figure 7E) produces ice fractions that resemble the [control-Control](#) case. We tested that adding the fall speed correction to explicit sedimentation does not matter (not shown).

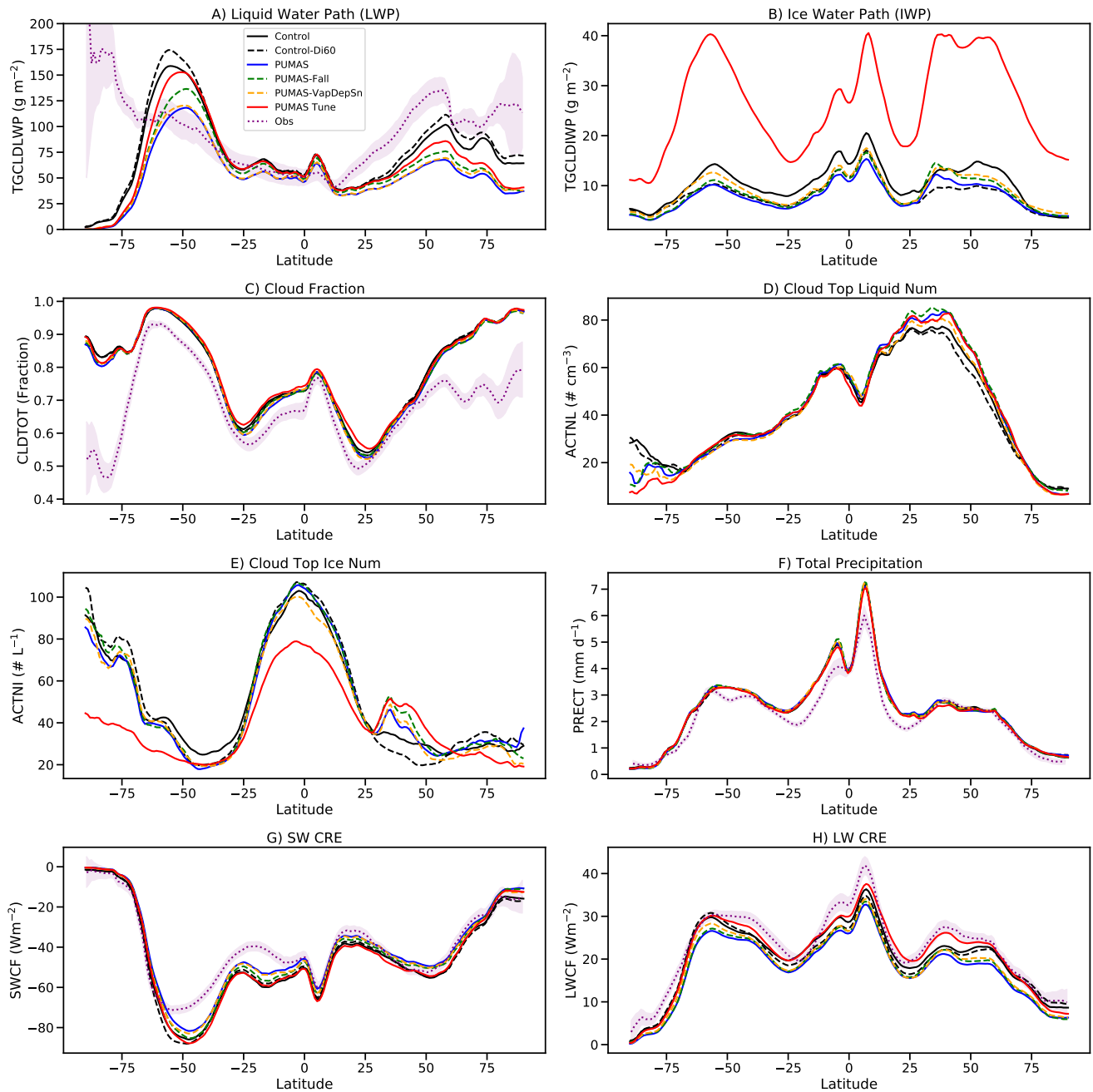


Figure 6. Zonal mean annual averages from 8-6 year global simulations for the MG3 Control (Black), PUMAS (Blue), PUMAS-VapDepSn (Green), PUMAS-Implicit (Orange) and PUMAS-Tune (Red). Simulation names are defined in Table 1. Also shown is the CERES EBAF climatology (purple) with 1 standard deviation of annual means: A) liquid water path (LWP), B) ice water path (IWP), C) cloud fraction, D) cloud top liquid number, E) cloud top drop number, F) total precipitation, G) shortwave (SW) cloud radiative effect (CRE), and H) longwave (LW) CRE.

Table 2. Global average kernel adjusted Cloud Feedback (CF) in $\text{W m}^{-2} \text{K}^{-1}$.

Run	Net CF	LW CF	SW CF
Control	0.59	0.15	0.44
Control-Di60	0.65	0.19	0.46
PUMAS	0.62 <u>0.65</u>	0.10	0.52 <u>0.55</u>
PUMAS-VapDepSn	0.64 <u>0.63</u>	0.09 <u>0.11</u>	0.54 <u>0.52</u>
PUMAS-Implicit <u>PUMAS-Fall</u>	0.56	0.11 <u>0.13</u>	0.46 <u>0.42</u>
PUMAS-Tune	0.67 <u>0.58</u>	0.06 <u>0.03</u>	0.61

380 The sedimentation likely impacts the evolution of ice near the freezing level. There are also some impacts at high latitudes. The tuning of clouds to increase liquid and ice water path modifies the ice fraction due to substantial differences in the liquid and ice water path (Figure 6), generally resulting in more moderate changes to ice fraction relative to the ~~control~~Control than with the standard PUMAS (with less condensate mass, Figure 7C).

4.4 Cloud Feedback

385 Cloud feedback is determined using a kernel adjusted cloud radiative forcing, as described by Soden et al. (2008), and implemented in CESM by Gettelman et al. (2012) (also used by Gettelman et al., 2019b).

Figure 8 illustrates the kernel adjusted cloud feedback estimates, weighted by the cosine of latitude (so that the ~~integral area~~integral area under the curve is the contribution to the global mean). Table 2 presents the global averages. PUMAS slightly increases the cloud feedback, lowering the LW and increasing the SW. Some of this results from the change to the detrained ice size (Control-Di60), not PUMAS itself. The ~~PUMAS-Implicit~~PUMAS-Fall SW feedbacks are very close to the Control-Di60 case, indicating that differences in SW feedbacks are perhaps due to the implicit sedimentation. The change to the fall speed was tested with explicit sedimentation and does not impact feedbacks. The mechanism might be through the changes to the ice phase seen in Figure 7. Net cloud feedback (Figure 8C) is reduced from 30–70° latitude in both hemispheres, but offset with changes at higher latitudes. The PUMAS-Tune simulation with enhanced cloud water has larger ~~cloud feedbacks, increased~~cloud feedbacks, increased ~~mostly in the SW and in the Southern Hemisphere mid-latitudes~~SW cloud feedbacks from 30°S–30°N, but some offsetting lower LW feedbacks. This is likely due to the significantly larger ice mass changing high (cirrus) cloud feedbacks, as LW feedbacks are lower in the tropics in regions of higher ice mass and number from 20–40°N (Figure 6).

We have examined maps of cloud feedback by regime for the LW and SW feedbacks, and there do not appear to be large and significant systematic differences in cloud feedback between the ~~control~~Control and PUMAS simulations. On the whole, 400 the impact of PUMAS on cloud feedbacks is moderate and not significant.

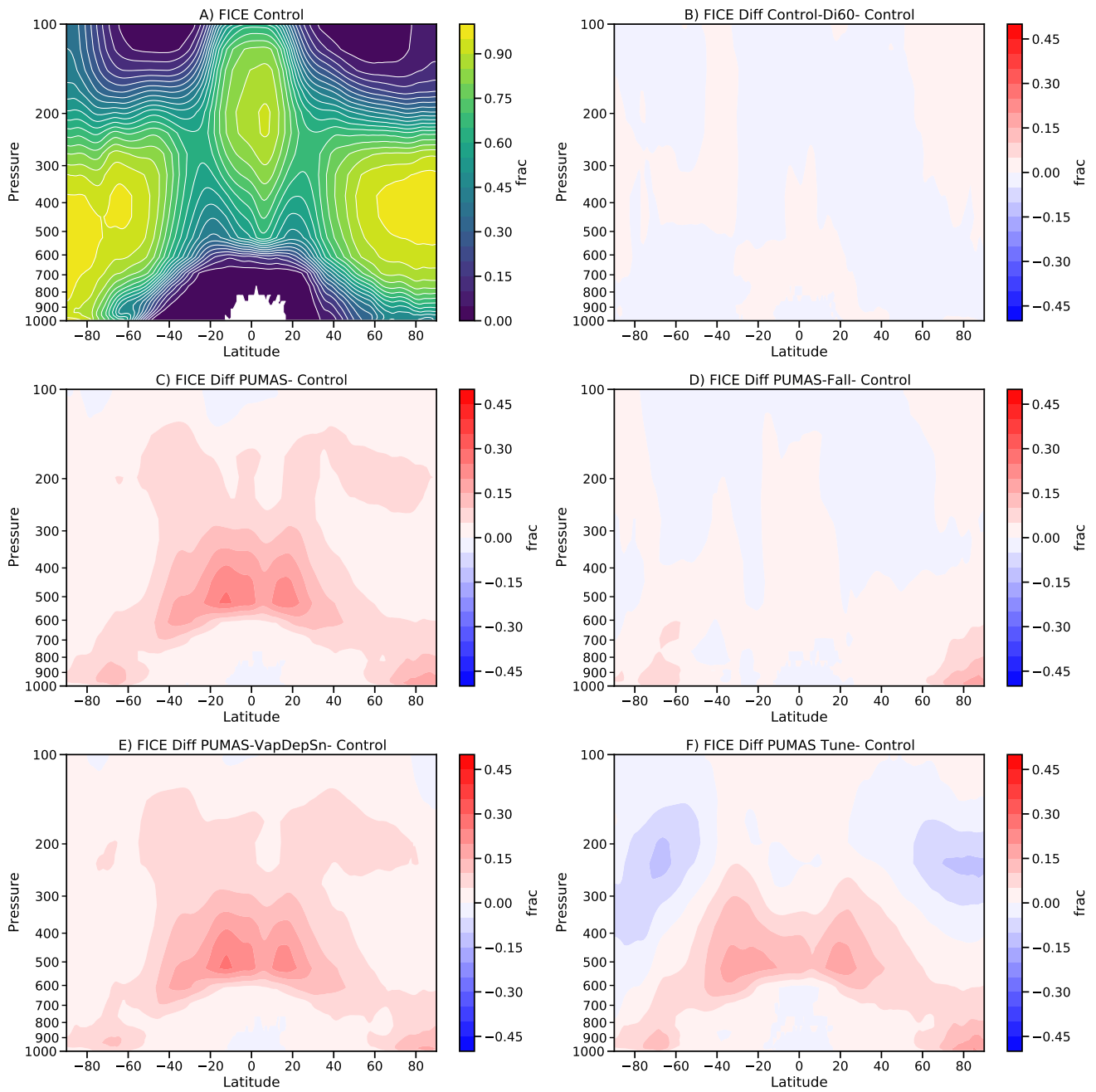


Figure 7. Zonal annual mean ice fraction for A) Control (MG3) and differences in ice fraction for B) Control-Di60 - Control, C) PUMAS - Control, D) PUMAS-VapDepSn - Control, E) PUMAS-Implicit - Control, and F) PUMAS Tune - Control. Simulation names are defined in Table 1.

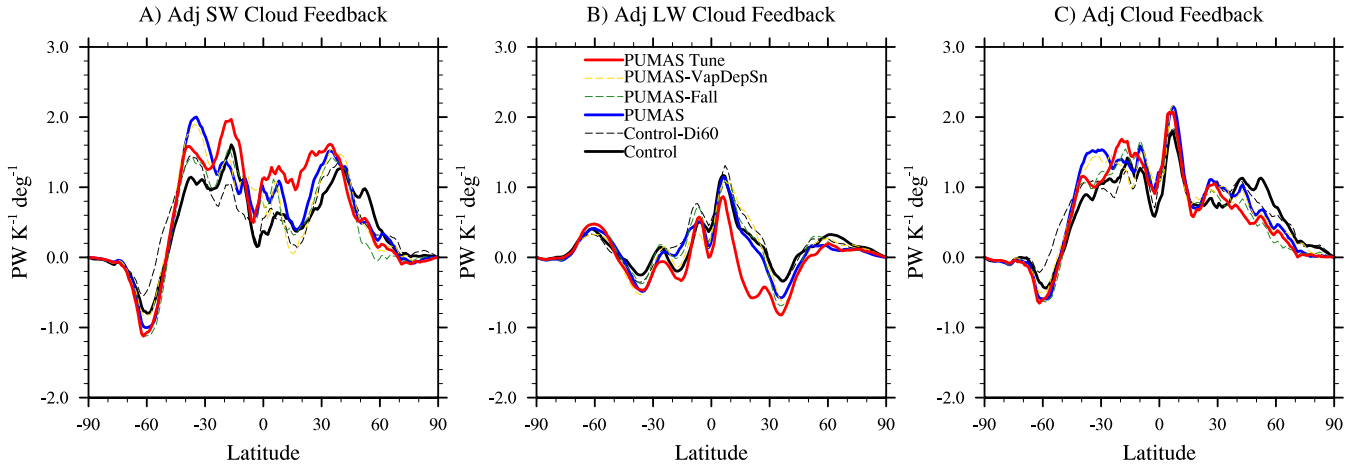


Figure 8. Zonal mean cloud feedback from SST+4K simulations: Control (Black), Control-Di60 (Black dashed) PUMAS (blue), PUMAS-Tune (red), PUMAS-VapDepSn (green dotted) and PUMAS-Implicit (orange dash). Simulation names are defined in Table 1. Feedbacks use kernel adjusted cloud radiative effects as described in Gettelman et al. (2013) and Gettelman et al. (2019b). Results are shown for A) SW Cloud Feedback, B) LW Cloud Feedback, and C) Net (LW+SW) Cloud Feedback.

4.5 Aerosol Forcing

Finally, we assess the impact of the changes in cloud microphysics on the aerosol forcing of climate by running 6 year simulations identical to the present day (PD) simulations, but with aerosol emissions set to 1850 emissions: ‘Pre-Industrial’ (PI). The difference PD–PI represents the impact of aerosols on climate. The indirect effect of aerosols on clouds is illustrated by the change in Cloud Radiative Effect (ΔCRE). For liquid clouds this is mostly in the SW (ΔSWCRE), and for ice clouds both the SW and LW (ΔLWCRE). The direct radiative effect of aerosols is the clearsky shortwave flux change (ΔSW_{clr}). The total effect is the all sky Residual Top Of Model (ΔRESTOM) flux change. Changes in column drop number (ΔCDNC) and Liquid Water Path (ΔLWP) and Ice Water Path (ΔIWP) are also assessed, which drive changes in CRE for clouds with liquid. For all quantities, the [global average](#) PD–PI differences are larger than twice the interannual standard deviation of global means of these quantities.

[The CAM6 total radiative effect due to aerosols \(\$\Delta\text{RESTOM}\$ \) is on high end of the range assessed by Bellouin et al. \(2020\)](#). Overall, the net aerosol forcing in present day (PD-PI) defined by ΔRESTOM drops by less than 10% with the PUMAS modifications (Table 3). This occurs due to [significant \(50%\) small](#) reductions in the negative SW clearsky forcing (direct effects of aerosols) and [20% small](#) reductions in SW cloud radiative effect changes, but is partially offset by [50%](#) reductions in the positive LW forcing as well. Thus, the magnitude of the components is [slightly](#) reduced. The PD-PI percent change in LWP

Table 3. Global average forcing change due to aerosol: PD-PI (W m^{-2}).

Run	ΔLWP	ΔIWP	ΔCLD	ΔCDNC	ΔSWCRE	ΔLWCRE	ΔSW_{clr}	ΔRESTOM
Units	%	g m^{-2}	%	%	Wm^{-2}	Wm^{-2}	Wm^{-2}	Wm^{-2}
Control	6.4 <u>6.0</u>	0.19	0.60	41 <u>29</u>	-2.3	0.53	-0.35	-1.9
Control-Di60	5.8 <u>5.5</u>	0.21	0.40	40 <u>29</u>	-2.2	0.63	-0.31	-1.8
PUMAS	6.2 <u>5.1</u>	-0.65 <u>-0.12</u>	0.40 <u>0.51</u>	41 <u>27</u>	-1.9 <u>-2.1</u>	0.22 <u>0.42</u>	-0.17 <u>-0.33</u>	-1.8
PUMAS-VapDepSn	6.6 <u>4.5</u>	-0.67 <u>-0.21</u>	0.28 <u>0.40</u>	41 <u>27</u>	-2.1	0.37 <u>0.47</u>	-0.19 <u>-0.27</u>	-1.9 <u>-1.7</u>
PUMAS-Implicit <u>PUMAS-Fall</u>	6.9 <u>5.3</u>	-0.87 <u>-0.18</u>	0.41 <u>0.55</u>	41 <u>28</u>	-2.1 <u>-2.3</u>	0.15 <u>0.50</u>	-0.21 <u>-0.28</u>	-2.0 <u>-1.8</u>
PUMAS-Tune	6.0 <u>4.1</u>	-3.08 <u>0.49</u>	0.28 <u>0.44</u>	36 <u>25</u>	-1.5 <u>-2.1</u>	-0.23 <u>0.64</u>	-0.23 <u>-0.13</u>	-1.9 <u>-1.3</u>

is similar, but IWP goes from an increase to a small decrease. The percent change in LWP is about 6% (increase in present) and lower with PUMAS than the control (Table 3). Cloud drop number increases by ~~40~~30%, while cloud fraction increases by less than 1%. The simulations are similar for the different sensitivity tests, but this masks regional differences.

Figure 9 illustrates the zonal mean changes in key quantities between pairs of PD and PI simulations. The gross aerosol forcing of climate in the SW (Figure 9A) and LW (Figure 9B) is ~~significantly reduced (closer to zero) in all~~ similar in most of the PUMAS simulations compared to the ~~control~~Control: SW forcing is negative and gets less so in the N. Hemisphere. LW forcing ~~goes from positive in the control simulation to near zero in~~ is reduced in all three PUMAS configurations, ~~and negative in~~ and the PUMAS-Tune simulation, ~~possibly due to decreases in IWP (Figure 9E)~~. The residual net change in top of model (TOM) flux, Figure 9C, has a lower magnitude (less negative) than the ~~control~~Control in N. Hemisphere high latitudes for the PUMAS Tune simulations (Figure 9C). There is a significant reduction in the LWP and column cloud drop number (CDNUMC) response from 25–90°N latitude (Figure 9D and F) which drives the reductions in the magnitude of the SW CRE changes (Figure 9A). Some of the difference is due to smaller mean values. The percent change in LWP is reduced in PUMAS simulations (Table 3), but the percent change in drop number is similar, except for the PUMAS Tune simulation.

Since the forcing response of most of the PUMAS simulations are similar, Figure 10 compares maps of the patterns of differences (PD-PI) for the Control (left column) and PUMAS (right column) simulations. Maps of the pattern of differences in Figure 10 show ~~clearly~~ that these changes occur in most places across the globe. SW CRE changes (Figure 10A and B) are reduced with PUMAS slightly throughout the N. Hemisphere, and even into the S. Hemisphere. ~~They are positive~~ There are some positive values over North East Asia. Changes are similar over the Pacific, with large impacts in the Eastern Pacific that is a common feature of CAM ACI effects, but lower in PUMAS. The LW CRE changes (Figure 10 C and D) have more ~~negative~~ positive values (Figure 10D) than the Control simulation (Figure 10C), especially over ~~East Asia, corresponding to the SW changes. Further analysis indicates this is due to a large decrease in IWP in this region in the PUMAS simulations (indicated in Figure 9E from 30–60°N). However, N.E. Asia has little impact on the TOM residual changes as a result of the offsetting effects (Figure 10 E and F)~~ the Indian Ocean, shifted from the Eastern Pacific, with little net effect. The LWP changes (Figure 10G and H) are smaller with PUMAS and localized closer to the source regions compared to the Control. This is true

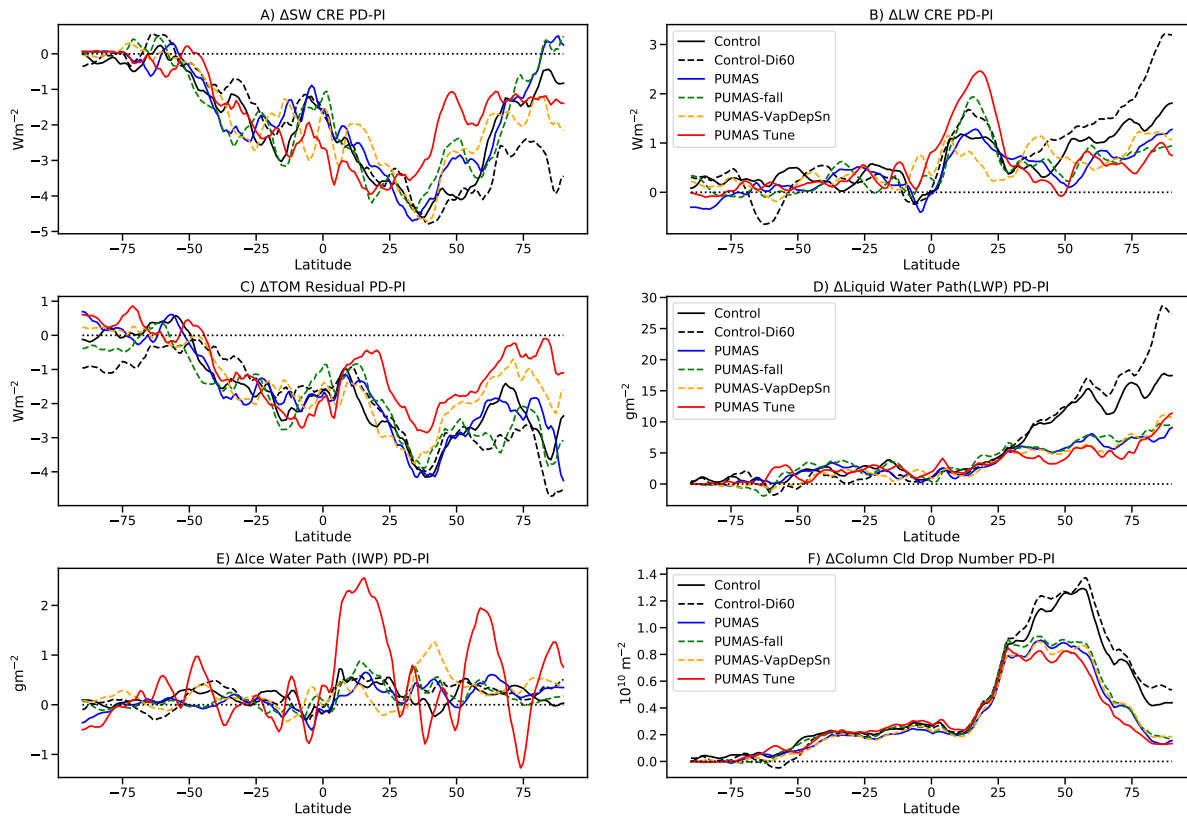


Figure 9. Zonal mean differences between ~~control~~Control (PD) and 1850 aerosol (PI) simulations for 4 pairs of runs: Control (Black), Control-Di60 (Black dash), PUMAS (blue), PUMAS-VapDepSn (green dash), PUMAS-Implicit (orange dash) and PUMAS Tune (red). Simulation names are defined in Table 1. Results are shown for A) change in SWCRE, B) change in LWCRE, C) change in net TOA flux (RESTOM), D) change in LWP, E) change in IWP, and F) change in column drop number.

440 especially in the Arctic (Figure 10H). Some of this is due to lower mean values, but the percent change in LWP is smaller (Table 3), and high latitude LWP is reduced in PUMAS (Figure 6A).

5 Discussion and Summary

We have described several adjustments to the MG3 cloud microphysical scheme now renamed PUMAS, including ~~removal~~ refactoring of an ice number limiter, adjustments to the fall speed calculation and use of an implicit numerical method for sedimentation, the addition of a process (vapor deposition onto snow), and the adjustment of accretion and the aerosol numbers input to the immersion freezing calculation.

445

The vapor deposition onto snow process has no significant effect on the simulations. Neither does the fall speed correction, even with explicit sedimentation (we do not expect much impact with implicit sedimentation). The major impact on the

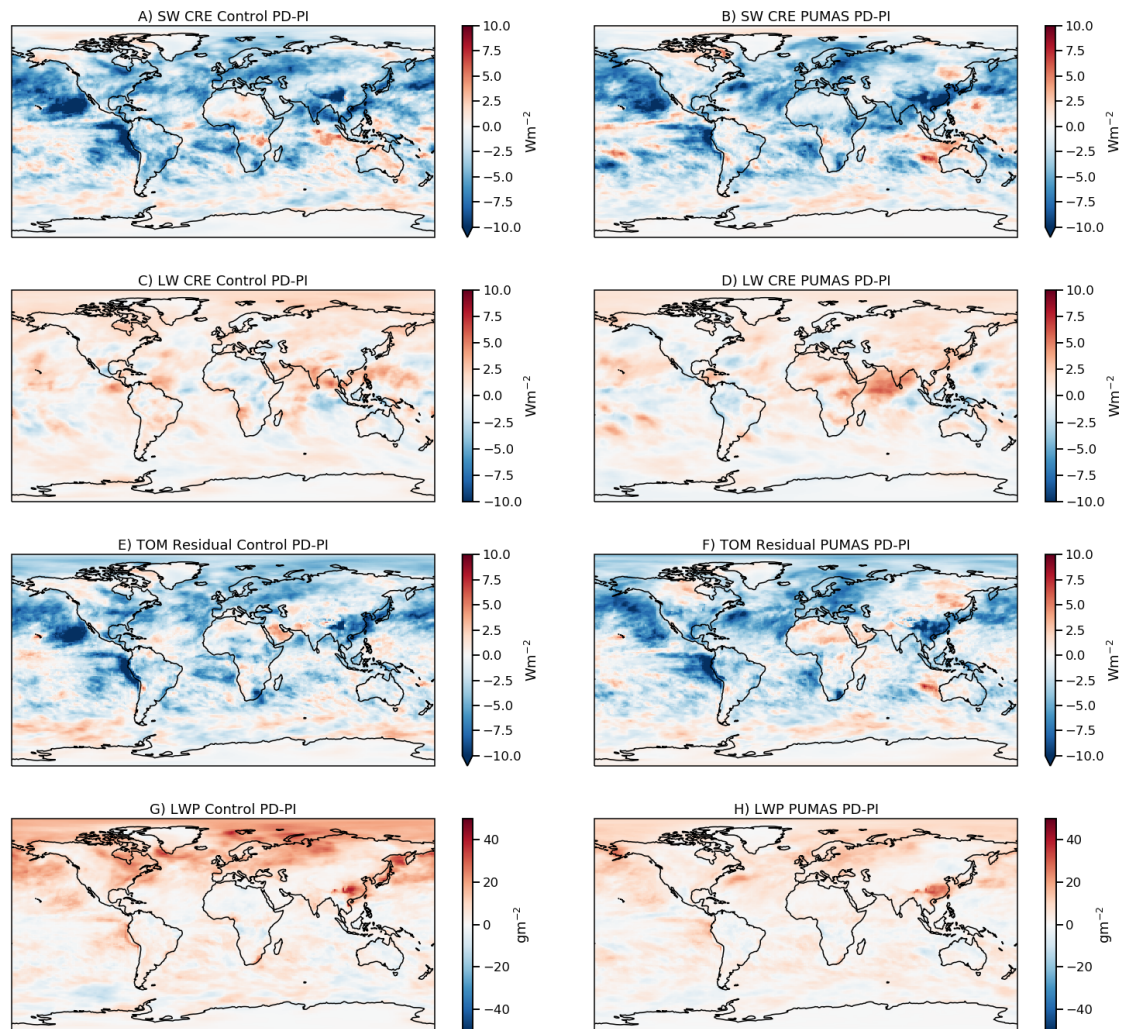


Figure 10. Differences between present day (PD) and 1850 aerosol (PI) simulations for Control (Left-A,C,E,G) and PUMAS+Accre (Right-B,D,F,H). Variables shown are A,B) SW Cloud Radiative Effect (SW CRE), C,D) LW Cloud Radiative Effect (LW CRE), E,F) Top of Model (TOM) Residual energy balance, and G,H) Liquid Water Path (LWP).

simulations comes from both the ~~removal-refactoring~~ of the ice number limiter (NIMAX), ice nucleation and the implicit
450 sedimentation.

The following is a summary of the main results:

1. GPU enabled microphysics code is significantly faster than the CPU version if a large number of columns can be loaded onto GPU accelerator chips. This results in a $2\times$ to $3\times$ speedup, with even more possibility for speed up at higher column counts. This would facilitate running at higher horizontal resolution.
- 455 2. ~~Removal-Refactoring~~ of the ice number limiter (change 1) results in extremely high ice numbers due to the CNT formulation of Immersion Freezing in CAM6. This significant increase in ice number is anomalous and creates a different climate state. This necessitated ~~switching back to immersion freezing based on size and temperature for cloud drops adjusting the aerosol numbers and dust in particular used in immersion freezing~~ (change 2), ~~as is done in all simulations for immersion freezing of rain~~. This might affect the solutions of Zhu et al. (2022), who removed the ice number limiter
460 but used a smaller microphysical timestep to control the unrealistic growth of ice number. One important message is that ice nucleation can have important climate effects.
3. The new PUMAS code reduces overall LWP and IWP. It is not clear what processes may be responsible for this as it occurs in all PUMAS simulations. The increase in accretion might be partially responsible, as well as the increased sedimentation limiting evaporation. The code can be adjusted to keep more condensed water path by reducing loss rates
465 for liquid and ice, as performed in the ‘Tune’ experiment.
4. The new PUMAS code reduces the aerosol forcing magnitudes ~~significantly~~slightly, with offsetting effects on the total ACI. The mechanism may be related to higher ice numbers and less liquid water at high latitudes. There is little net change on aerosol forcing, but reductions in magnitude of SW and LW components.
5. The PUMAS changes have small impacts on cloud feedbacks and climate sensitivity. There are reductions in the
470 N. Hemisphere mid-latitude feedbacks and increases in the S. Hemisphere midlatitudes. Tropical feedbacks increase slightly. Feedback changes appear to be due mainly to the implicit sedimentation (~~changes~~change 5); reverting this change makes PUMAS look more like the ~~control~~Control.
6. The implicit sedimentation calculation (~~changes~~change 5) also ~~contribute~~contributes to lowering the aerosol forcing, likely through changes to precipitation production, with less change to LWP. The implicit sedimentation reduces sensi-
475 tivity to the time step and increases the ice fraction near the freezing level. There does not seem to be an appreciable difference in the time-averaged precipitation or the precipitation process rates due to use of a less accurate implicit method.

Next steps for PUMAS development include integrating the unified ice formulation of Eidhammer et al. (2016), further investigations into ice nucleation and the budget of ~~ice nuclei~~INP, and the exploration of flexible form to the size distribu-
480 tions (Morrison et al., 2020). In addition, the GPU results motivate further work to add GPU directives to all the physical parameterizations in CAM.

Code and data availability. The updated model code described here is available in the PUMAS Repository <https://github.com/ESCOMP/PUMAS> as implemented in the Community Atmosphere model <https://github.com/ESCOMP/CAM>. Derived data sets in CAM and SCAM are available at [doi:10.5281/zenodo.7105927](https://doi.org/10.5281/zenodo.7105927). https://github.com/ESCOMP/PUMAS/tree/pumas_cam-release_v1.27 as implemented in the Community Atmosphere model https://github.com/ESCOMP/CAM/tree/cam6_3_075. Derived data sets in CAM and SCAM as well as an archived version of the repository code are available at [doi:10.5281/zenodo.7579707](https://doi.org/10.5281/zenodo.7579707).

Author contributions. AG performed simulations and wrote the manuscript. TE and KT-C helped develop and integrate the code. HM assisted with code modifications and editing of the manuscript. JS and JD worked on the GPU code. ZM found the original issues with ice nucleation and helped analyze solutions with TS. RF assisted with discussions of numerics and implicit sedimentation compared to other models. JZ helped develop and test some of the changes to ice nucleation.

Competing interests. I declare that no competing interests are present.

Acknowledgements. [The National Center for Atmospheric Research is supported by the U. S. National Science Foundation. The Pacific Northwest National Laboratory is operated by Battelle for the U. S. Department of Energy. Thanks to Simone Tilmes for sharing ideas about correcting the Immersion Freezing.](#)

- Abdul-Razzak, H. and Ghan, S. J.: A Parameterization of Aerosol Activation 3. Sectional Representation, *J. Geophys. Res.*, 107, AAC 1–1 – AAC 1–6, <https://doi.org/10.1029/2001JD000483>, 2002.
- Adler, R. F., Sapiano, M. R. P., Huffman, G. J., Wang, J.-J., Gu, G., Bolvin, D., Chiu, L., Schneider, U., Becker, A., Nelkin, E., Xie, P., Ferraro, R., and Shin, D.-B.: The Global Precipitation Climatology Project (GPCP) Monthly Analysis (New Version 2.3) and a Review of
500 2017 Global Precipitation, *Atmosphere*, 9, 138, <https://doi.org/10.3390/atmos9040138>, 2018.
- Barahona, D., Molod, A., Bacmeister, J., Nenes, A., Gettelman, A., Morrison, H., Phillips, V., and Eichmann, A.: Development of Two-Moment Cloud Microphysics for Liquid and Ice within the NASA Goddard Earth Observing System Model (GEOS-5), *Geoscientific Model Development*, 7, 1733–1766, <https://doi.org/10.5194/gmd-7-1733-2014>, 2014.
- Bellouin, N., Quaas, J., Gryspeerdt, E., Kinne, S., Stier, P., Watson-Parris, D., Boucher, O., Carslaw, K. S., Christensen, M., Daniau, A.-
505 L., Dufresne, J.-L., Feingold, G., Fiedler, S., Forster, P., Gettelman, A., Haywood, J. M., Lohmann, U., Malavelle, F., Mauritsen, T., McCoy, D. T., Myhre, G., Mülmenstädt, J., Neubauer, D., Possner, A., Rugenstein, M., Sato, Y., Schulz, M., Schwartz, S. E., Sourdeval, O., Storelvmo, T., Toll, V., Winker, D., and Stevens, B.: Bounding Global Aerosol Radiative Forcing of Climate Change, *Reviews of Geophysics*, 58, e2019RG000 660, <https://doi.org/10.1029/2019RG000660>, 2020.
- Bigg, E. K.: The Formation of Atmospheric Ice Crystals by the Freezing of Droplets, *qjrms*, 79, 510–519, 1953.
- 510 Bodas-Salcedo, A., Mulcahy, J. P., Andrews, T., Williams, K. D., Ringer, M. A., Field, P. R., and Elsaesser, G. S.: Strong Dependence of Atmospheric Feedbacks on Mixed-Phase Microphysics and Aerosol-Cloud Interactions in HadGEM3, *Journal of Advances in Modeling Earth Systems*, 11, 1735–1758, <https://doi.org/10.1029/2019MS001688>, 2019.
- Bogenschutz, P. A., Gettelman, A., Morrison, H., Larson, V. E., Craig, C., and Schanen, D. P.: Higher-Order Turbulence Closure and Its Impact on Climate Simulation in the Community Atmosphere Model, *Journal of Climate*, 26, 9655–9676, [https://doi.org/10.1175/JCLI-](https://doi.org/10.1175/JCLI-D-13-00075.1)
515 D-13-00075.1, 2013.
- Cesana, G., Genio, A. D. D., Ackerman, A. S., Kelley, M., Elsaesser, G., Fridlind, A. M., Cheng, Y., and Yao, M.-S.: Evaluating Models' Response of Tropical Low Clouds to SST Forcings Using CALIPSO Observations, *Atmospheric Chemistry and Physics*, 19, 2813–2832, <https://doi.org/10.5194/acp-19-2813-2019>, 2019.
- Cess, R. D. et al.: Interpretation of Cloud-Climate Feedback as Produced by 14 Atmospheric General Circulation Models, *Science*, 245,
520 513–516, 1989.
- Danabasoglu, G., Lamarque, J.-F., Bacmeister, J., Bailey, D. A., DuVivier, A. K., Edwards, J., Emmons, L. K., Fasullo, J., Garcia, R., Gettelman, A., Hannay, C., Holland, M. M., Large, W. G., Lauritzen, P. H., Lawrence, D. M., Lenaerts, J. T. M., Lindsay, K., Lipscomb, W. H., Mills, M. J., Neale, R., Oleson, K. W., Otto-Bliesner, B., Phillips, A. S., Sacks, W., Tilmes, S., van Kampenhout, L., Vertenstein, M., Bertini, A., Dennis, J., Deser, C., Fischer, C., Fox-Kemper, B., Kay, J. E., Kinnison, D., Kushner, P. J., Larson, V. E., Long, M. C.,
525 Mickelson, S., Moore, J. K., Nienhouse, E., Polvani, L., Rasch, P. J., and Strand, W. G.: The Community Earth System Model Version 2 (CESM2), *Journal of Advances in Modeling Earth Systems*, 12, e2019MS001 916, <https://doi.org/10.1029/2019MS001916>, 2020.
- Eidhammer, T., Morrison, H., Mitchell, D., Gettelman, A., and Erfani, E.: Improvements in Global Climate Model Microphysics Using a Consistent Representation of Ice Particle Properties, *J. Climate*, 30, 609–629, <https://doi.org/10.1175/JCLI-D-16-0050.1>, 2016.
- Forbes, R., Greer, A., Loniz, K., and Ahlgrimm, M.: Reducing Systematic Errors in Cold-Air Outbreaks, *ECMWF Newsletter*, pp. 17–22,
530 2015.

- Gottelman, A.: Putting the Clouds Back in Aerosol–Cloud Interactions, *Atmos. Chem. Phys.*, 15, 12 397–12 411, <https://doi.org/10.5194/acp-15-12397-2015>, 2015.
- Gottelman, A. and Morrison, H.: Advanced Two-Moment Bulk Microphysics for Global Models. Part I: Off-Line Tests and Comparison with Other Schemes, *Journal of Climate*, 28, 1268–1287, <https://doi.org/10.1175/JCLI-D-14-00102.1>, 2015.
- 535 Gottelman, A., Morrison, H., and Ghan, S. J.: A New Two-Moment Bulk Stratiform Cloud Microphysics Scheme in the NCAR Community Atmosphere Model (CAM3), Part II: Single-Column and Global Results, *Joc*, 21, 3660–3679, 2008.
- Gottelman, A., Liu, X., Ghan, S. J., Morrison, H., Park, S., Conley, A. J., Klein, S. A., Boyle, J., Mitchell, D. L., and Li, J.-L. F.: Global Simulations of Ice Nucleation and Ice Supersaturation with an Improved Cloud Scheme in the Community Atmosphere Model, *J. Geophys. Res.*, 115, <https://doi.org/10.1029/2009JD013797>, 2010.
- 540 Gottelman, A., Kay, J. E., and Shell, K. M.: The Evolution of Climate Feedbacks in the Community Atmosphere Model, *J. Climate*, 25, 1453–1469, <https://doi.org/10.1175/JCLI-D-11-00197.1>, 2012.
- Gottelman, A., Fasullo, J. T., and Kay, J. E.: Spatial Decomposition of Climate Feedbacks in the Community Earth System Model, *J. Climate*, 40, 3544–2561, <https://doi.org/10.1175/JCLI-D-12-00497.1>, 2013.
- Gottelman, A., Morrison, H., Santos, S., Bogenschutz, P., and Caldwell, P. M.: Advanced Two-Moment Bulk Microphysics for Global
- 545 Models. Part II: Global Model Solutions and Aerosol–Cloud Interactions, *J. Climate*, 28, 1288–1307, <https://doi.org/10.1175/JCLI-D-14-00103.1>, 2015.
- Gottelman, A., Lin, L., Medeiros, B., and Olson, J.: Climate Feedback Variance and the Interaction of Aerosol Forcing and Feedbacks, *J. Climate*, 29, 6659–6675, <https://doi.org/10.1175/JCLI-D-16-0151.1>, 2016.
- Gottelman, A., Hannay, C., Bacmeister, J. T., Neale, R. B., Pendergrass, A. G., Danabasoglu, G., Lamarque, J.-F., Fasullo, J. T., Bailey, D. A.,
- 550 Lawrence, D. M., and Mills, M. J.: High Climate Sensitivity in the Community Earth System Model Version 2 (CESM2), *Geophysical Research Letters*, 46, 8329–8337, <https://doi.org/10.1029/2019GL083978>, 2019a.
- Gottelman, A., Mills, M. J., Kinnison, D. E., Garcia, R. R., Smith, A. K., Marsh, D. R., Tilmes, S., Vitt, F., Bardeen, C. G., McInerny, J., Liu, H.-L., Solomon, S. C., Polvani, L. M., Emmons, L. K., Lamarque, J.-F., Richter, J. H., Glanville, A. S., Bacmeister, J. T., Phillips, A. S., Neale, R. B., Simpson, I. R., DuVivier, A. K., Hodzic, A., and Randel, W. J.: The Whole Atmosphere Community Climate Model Version
- 555 6 (WACCM6), *Journal of Geophysical Research: Atmospheres*, 124, 12 380–12 403, <https://doi.org/10.1029/2019JD030943>, 2019b.
- Gottelman, A., Morrison, H., Thayer-Calder, K., and Zarzycki, C. M.: The Impact of Rimed Ice Hydrometeors on Global and Regional Climate, *Journal of Advances in Modeling Earth Systems*, 0, <https://doi.org/10.1029/2018MS001488>, 2019c.
- Gottelman, A., Bardeen, C. G., McCluskey, C. S., Järvinen, E., Stith, J., Bretherton, C., McFarquhar, G., Twohy, C., D’Alessandro, J., and Wu, W.: Simulating Observations of Southern Ocean Clouds and Implications for Climate, *Journal of Geophysical Research: Atmospheres*,
- 560 125, e2020JD032 619, <https://doi.org/10.1029/2020JD032619>, 2020.
- Gottelman, A., Carmichael, G. R., Feingold, G., Silva, A. M. D., and van den Heever, S. C.: Confronting Future Models with Future Satellite Observations of Clouds and Aerosols, *Bulletin of the American Meteorological Society*, 102, E1557–E1562, <https://doi.org/10.1175/BAMS-D-21-0029.1>, 2021a.
- Gottelman, A., Lamboll, R., Bardeen, C. G., Forster, P. M., and Watson-Parris, D.: Climate Impacts of COVID-19 Induced Emission Changes, *Geophysical Research Letters*, 48, e2020GL091 805, <https://doi.org/10.1029/2020GL091805>, 2021b.
- 565 Golaz, J.-C., Larson, V. E., and Cotton, W. R.: A PDF-Based Model for Boundary Layer Clouds. Part II: Model Results, *J. Atmos. Sci.*, 59, 3552–3571, 2002.

- Gryspeerdt, E., Sourdeval, O., Quaas, J., Delanoë, J., Krämer, M., and Kühne, P.: Ice Crystal Number Concentration Estimates from Li-
dar–Radar Satellite Remote Sensing – Part 2: Controls on the Ice Crystal Number Concentration, *Atmospheric Chemistry and Physics*,
18, 14 351–14 370, <https://doi.org/10.5194/acp-18-14351-2018>, 2018.
- 570 Guo, H., Ming, Y., Fan, S., Zhou, L., Harris, L., and Zhao, M.: Two-Moment Bulk Cloud Microphysics With Prognostic Precipita-
tion in GFDL’s Atmosphere Model AM4.0: Configuration and Performance, *Journal of Advances in Modeling Earth Systems*, 13,
e2020MS002 453, <https://doi.org/10.1029/2020MS002453>, 2021.
- Harris, L., Zhou, L., Lin, S.-J., Chen, J.-H., Chen, X., Gao, K., Morin, M., Rees, S., Sun, Y., Tong, M., Xiang, B., Bender, M., Benson, R.,
575 Cheng, K.-Y., Clark, S., Elbert, O. D., Hazelton, A., Huff, J. J., Kaltenbaugh, A., Liang, Z., Marchok, T., Shin, H. H., and Stern, W.: GFDL
SHIELD: A Unified System for Weather-to-Seasonal Prediction, *Journal of Advances in Modeling Earth Systems*, 12, e2020MS002 223,
<https://doi.org/10.1029/2020MS002223>, 2020.
- Hoose, C. and Möhler, O.: Heterogeneous Ice Nucleation on Atmospheric Aerosols: A Review of Results from Laboratory Experiments,
Atmospheric Chemistry and Physics, 12, 9817–9854, <https://doi.org/10.5194/acp-12-9817-2012>, 2012.
- 580 Hoose, C., Kristjánsson, J. E., Chen, J.-P., and Hazra, A.: A Classical-Theory-Based Parameterization of Heterogeneous Ice
Nucleation by Mineral Dust, Soot, and Biological Particles in a Global Climate Model, *J. Atmos. Sci.*, 67, 2483–2503,
<https://doi.org/10.1175/2010JAS3425.1>, 2010.
- Hoyle, C., Luo, B., and Peter, T.: The Origin of High Ice Crystal Number Densities in Cirrus Clouds, *Journal of the atmospheric sciences*,
62, 2568–2579, 2005.
- 585 Hurrell, J. W., Hack, J. J., Shea, D., Caron, J. M., and Rosinski, J.: A New Sea Surface Temperature and Sea Ice Boundary Dataset for the
Community Atmosphere Model, *joc*, 21, 5145–5153, 2010.
- Iacono, M. J., Mlawer, E. J., Clough, S. A., and Morcrette, J.-J.: Impact of an Improved Longwave Radiation Model, RRTM, on the Energy
Budget and Thermodynamic Properties of the NCAR Community Climate Model, CCM3, *jgr*, 105, 14,873–14,890, 2000.
- Kanji, Z. A., Ladino, L. A., Wex, H., Boose, Y., Burkert-Kohn, M., Cziczo, D. J., and Krämer, M.: Overview of Ice Nucleating Particles,
590 *Meteorological Monographs*, 58, 1.1–1.33, <https://doi.org/10.1175/AMSMONOGRAPHS-D-16-0006.1>, 2017.
- Khairoutdinov, M. F. and Kogan, Y.: A New Cloud Physics Parameterization in a Large-Eddy Simulation Model of Marine Stratocumulus,
Monthly Weather Review, 128, 229–243, 2000.
- Larson, V. E., Golaz, J.-C., and Cotton, W. R.: Small-Scale and Mesoscale Variability in Cloudy Boundary Layers: Joint Probability Density
Functions, *J. Atmos. Sci.*, 59, 3519–3539, [https://doi.org/10.1175/1520-0469\(2002\)059<3519:SSAMVI>2.0.CO;2](https://doi.org/10.1175/1520-0469(2002)059<3519:SSAMVI>2.0.CO;2), 2002.
- 595 Lebsock, M., Morrison, H., and Gettelman, A.: Microphysical Implications of Cloud-Precipitation Covariance Derived from Satellite Remote
Sensing, *J. Geophys. Res.*, 118, 6521–6533, <https://doi.org/10.1002/jgrd.50347>, 2013.
- Liu, X. and Penner, J. E.: Ice Nucleation Parameterization for Global Models, *Meteor. Z.*, 14, 2005.
- Liu, X., Ma, P.-L., Wang, H., Tilmes, S., Singh, B., Easter, R. C., Ghan, S. J., and Rasch, P. J.: Description and Evaluation of a New Four-
Mode Version of the Modal Aerosol Module (MAM4) within Version 5.3 of the Community Atmosphere Model, *Geoscientific Model*
600 *Development*, 9, 505–522, <https://doi.org/10.5194/gmd-9-505-2016>, 2016.
- Loeb, N. G., Doelling, D. R., Wang, H., Su, W., Nguyen, C., Corbett, J. G., Liang, L., Mitrescu, C., Rose, F. G., and Kato, S.: Clouds and
the Earth’s Radiant Energy System (CERES) Energy Balanced and Filled (EBAF) Top-of-Atmosphere (TOA) Edition-4.0 Data Product,
J. Climate, 31, 895–918, <https://doi.org/10.1175/JCLI-D-17-0208.1>, 2018.
- Lohmann, U., Feichter, J., Chuang, C. C., and Penner, J.: Prediction of the Number of Cloud Droplets in the ECHAM GCM, *jgr*, 104,
605 9169–9198, 1999.

- Lohmann, U., Stier, P., Hoose, C., Ferrachat, S., Roeckner, E., and Zhang, J.: Cloud Microphysics and Aerosol Indirect Effects in the Global Climate Model ECHAM5-HAM, *Atmos. Chem. Phys.*, 7, 3245–3446, 2007.
- McGraw, Z., Storelvmo, T., Polvani, L. M., Hofer, S., Shaw, J. K., and Gettelman, A.: On the Links between Ice Nucleation, Cloud Phase, and Climate Sensitivity in CESM2, Preprint, Preprints, <https://doi.org/10.22541/essoar.167214452.25853014/v1>, 2022.
- 610 Meyers, M. P., DeMott, P. J., and Cotton, W. R.: New Primary Ice-Nucleation Parameterizations in an Explicit Cloud Model, *J. Applied Met.*, 31, 708–721, 1992.
- Michibata, T., Suzuki, K., Sekiguchi, M., and Takemura, T.: Prognostic Precipitation in the MIROC6-SPRINTARS GCM: Description and Evaluation Against Satellite Observations, *Journal of Advances in Modeling Earth Systems*, 11, 839–860, <https://doi.org/10.1029/2018MS001596>, 2019.
- 615 Milbrandt, J. A. and Yau, M. K.: A Multimoment Bulk Microphysics Parameterization. Part I: Analysis of the Role of the Spectral Shape Parameter, *J. Atmos. Sci.*, 62, 3051–3064, <https://doi.org/10.1175/JAS3534.1>, 2005.
- Morrison, H. and Gettelman, A.: A New Two-Moment Bulk Stratiform Cloud Microphysics Scheme in the NCAR Community Atmosphere Model (CAM3), Part I: Description and Numerical Tests, *J. Climate*, 21, 3642–3659, 2008.
- Morrison, H. and Milbrandt, J. A.: Parameterization of Cloud Microphysics Based on the Prediction of Bulk Ice Particle Properties. Part
620 I: Scheme Description and Idealized Tests, *Journal of the Atmospheric Sciences*, 72, 287–311, <https://doi.org/10.1175/JAS-D-14-0065.1>, 2015.
- Morrison, H., Curry, J. A., and Khvorostyanov, V. I.: A New Double-Moment Microphysics Parameterization for Application in Cloud and Climate Models. Part I: Description, *jas*, 62, 1665–1677, 2005.
- Morrison, H., van Lier-Walqui, M., Fridlind, A. M., Grabowski, W. W., Harrington, J. Y., Hoose, C., Korolev, A., Kumjian, M. R., Mil-
625 brandt, J. A., Pawlowska, H., Posselt, D. J., Prat, O. P., Reimel, K. J., Shima, S.-I., van Dienenhoven, B., and Xue, L.: Confronting the Challenge of Modeling Cloud and Precipitation Microphysics, *Journal of Advances in Modeling Earth Systems*, 12, e2019MS001689, <https://doi.org/10.1029/2019MS001689>, 2020.
- Neale, R. B., Richter, J. H., and Jochum, M.: The Impact of Convection on ENSO: From a Delayed Oscillator to a Series of Events, *J. Climate*, 21, 5904–, <https://doi.org/10.1175/2008JCLI2244.1>, 2008.
- 630 Rutan, D. A., Kato, S., Doelling, D. R., Rose, F. G., Nguyen, L. T., Caldwell, T. E., and Loeb, N. G.: CERES Synoptic Product: Methodology and Validation of Surface Radiant Flux, *Journal of Atmospheric and Oceanic Technology*, 32, 1121–1143, <https://doi.org/10.1175/JTECH-D-14-00165.1>, 2015.
- Salzmann, M., Ming, Y., Golaz, J.-C., Ginoux, P. A., Morrison, H., Gettelman, A., Krämer, M., and Donner, L. J.: Two-Moment Bulk Stratiform Cloud Microphysics in the GFDL AM3 GCM: Description, Evaluation, and Sensitivity Tests, *acp*, 10, 8037–8064,
635 <https://doi.org/10.5194/acp-10-8037-2010>, 2010.
- Santos, S. P., Caldwell, P. M., and Bretherton, C. S.: Numerically Relevant Timescales in the MG2 Microphysics Model, *Journal of Advances in Modeling Earth Systems*, n/a, e2019MS001972, <https://doi.org/10.1029/2019MS001972>, 2020.
- Shaw, J., McGraw, Z. S., Bruno, O., Storelvmo, T., and Hofer, S.: Using Satellite Observations to Evaluate Model Microphysical Representation of Arctic Mixed-Phase Clouds, *Geophysical Research Letters*, n/a, e2021GL096191, <https://doi.org/10.1029/2021GL096191>,
640 2022.
- Shaw, J. K., McGraw, Z., Bruno, O., Storelvmo, T., and Hofer, S.: Using Satellite Observations to Evaluate Model Representation of Arctic Mixed-Phase Clouds, <http://www.essoar.org/doi/10.1002/essoar.10506728.1>, <https://doi.org/10.1002/essoar.10506728.1>, 2021.

- Sherwood, S., Webb, M. J., Annan, J. D., Armour, K. C., Forster, P. M., Hargreaves, J. C., Hegerl, G., Klein, S. A., Marvel, K. D., Rohling, E. J., Watanabe, M., Andrews, T., Braconnot, P., Bretherton, C. S., Foster, G. L., Hausfather, Z., von der Heydt, A. S., Knutti, R., Mauritsen, T., Norris, J. R., Proistosescu, C., Rugenstein, M., Schmidt, G. A., Tokarska, K. B., and Zelinka, M. D.: An Assessment of Earth's Climate Sensitivity Using Multiple Lines of Evidence, *Reviews of Geophysics*, n/a, e2019RG000678, <https://doi.org/10.1029/2019RG000678>, 2020.
- 645 Shi, X., Liu, X., and Zhang, K.: Effects of Pre-Existing Ice Crystals on Cirrus Clouds and Comparison between Different Ice Nucleation Parameterizations with the Community Atmosphere Model (CAM5), *Atmospheric Chemistry and Physics*, 15, 1503–1520, <https://doi.org/10.5194/acp-15-1503-2015>, 2015.
- Shipway, B. J. and Hill, A. A.: Diagnosis of Systematic Differences between Multiple Parametrizations of Warm Rain Microphysics Using a Kinematic Framework, *Quarterly Journal of the Royal Meteorological Society*, 138, 2196–2211, <https://doi.org/10.1002/qj.1913>, 2012.
- Soden, B. J., Held, I. M., Colman, R., Shell, K. M., Kiehl, J. T., and Shields, C. A.: Quantifying Climate Feedbacks Using Radiative Kernels, *J. Climate*, 21, 3504–3520, <https://doi.org/10.1175/2007JCLI2110.1>, 2008.
- 655 Sourdeval, O., Gryspeerdt, E., Krämer, M., Goren, T., Delanoë, J., Afchine, A., Hemmer, F., and Quaas, J.: Ice Crystal Number Concentration Estimates from Lidar–Radar Satellite Remote Sensing – Part I: Method and Evaluation, *Atmospheric Chemistry and Physics*, 18, 14327–14350, <https://doi.org/10.5194/acp-18-14327-2018>, 2018.
- Stephens, G. L., L'Ecuyer, T., Forbes, R., Gettelman, A., Golaz, J.-C., Bodas-Salcedo, A., Suzuki, K., Gabriel, P., and Haynes, J.: Dreary State of Precipitation in Global Models, *JGR*, 115, <https://doi.org/10.1029/2010JD014532>, 2010.
- 660 Sun, J., Fu, J. S., Drake, J. B., Zhu, Q., Haidar, A., Gates, M., Tomov, S., and Dongarra, J.: Computational Benefit of GPU Optimization for the Atmospheric Chemistry Modeling, *Journal of Advances in Modeling Earth Systems*, 10, 1952–1969, <https://doi.org/10.1029/2018MS001276>, 2018.
- Tan, I. and Storelvmo, T.: Evidence of Strong Contributions From Mixed-Phase Clouds to Arctic Climate Change, *Geophysical Research Letters*, 46, 2894–2902, <https://doi.org/10.1029/2018GL081871>, 2019.
- 665 Tan, I., Storelvmo, T., and Zelinka, M. D.: Observational Constraints on Mixed-Phase Clouds Imply Higher Climate Sensitivity, *Science*, 352, 224–227, <https://doi.org/10.1126/science.aad5300>, 2016.
- Thompson, G. and Eidhammer, T.: A Study of Aerosol Impacts on Clouds and Precipitation Development in a Large Winter Cyclone, *J. Atmos. Sci.*, 71, 3636–3658, <https://doi.org/10.1175/JAS-D-13-0305.1>, 2014.
- Twomey, S.: The Influence of Pollution on the Shortwave Albedo of Clouds, *Journal of the Atmospheric Sciences*, 34, 1149–1152, 1977.
- 670 Worley, P. H. and Drake, J. B.: Performance Portability in the Physical Parameterizations of the Community Atmosphere Model, *The International Journal of High Performance Computing Applications*, 19, 187–201, <https://doi.org/10.1177/1094342005056095>, 2005.
- Zelinka, M. D., Myers, T. A., McCoy, D. T., Po-Chedley, S., Caldwell, P. M., Ceppi, P., Klein, S. A., and Taylor, K. E.: Causes of Higher Climate Sensitivity in CMIP6 Models, *Geophysical Research Letters*, 47, e2019GL085782, <https://doi.org/10.1029/2019GL085782>, 2020.
- Zhang, G. J. and McFarlane, N. A.: Sensitivity of Climate Simulations to the Parameterization of Cumulus Convection in the Canadian Climate Center General Circulation Model, *Atmos. Ocean*, 33, 407–446, 1995.
- 675 Zhao, X., Lin, Y., Peng, Y., Wang, B., Morrison, H., and Gettelman, A.: A Single Ice Approach Using Varying Ice Particle Properties in Global Climate Model Microphysics, *J. Adv. Model. Earth Syst.*, pp. n/a–n/a, <https://doi.org/10.1002/2017MS000952>, 2017.
- Zhou, L., Lin, S.-J., Chen, J.-H., Harris, L. M., Chen, X., and Rees, S. L.: Toward Convective-Scale Prediction within the Next Generation Global Prediction System, *Bulletin of the American Meteorological Society*, 100, 1225–1243, <https://doi.org/10.1175/BAMS-D-17-0246.1>, 2019.
- 680

Zhu, J., Otto-Bliesner, B. L., Brady, E. C., Gettelman, A., Bacmeister, J. T., Neale, R. B., Poulsen, C. J., Shaw, J. K., McGraw, Z. S., and Kay, J. E.: LGM Paleoclimate Constraints Inform Cloud Parameterizations and Equilibrium Climate Sensitivity in CESM2, *Journal of Advances in Modeling Earth Systems*, 14, e2021MS002776, <https://doi.org/10.1029/2021MS002776>, 2022.